DOKUZ EYLÜL UNIVERSITY

GRADUATE SCHOOL OF NATURAL AND APPLIED SCIENCES

PRODUCTION AND APPLICATION OF PHOTOCATALYSTS FOR DETOXIFICATION OF CONTAMINATED WATER

by

Güneş KURŞUN

June, 2015

İZMİR

PRODUCTION AND APPLICATION OF PHOTOCATALYSTS FOR DETOXIFICATION OF CONTAMINATED WATER

A Thesis Submitted to the
Graduate School of Natural and Applied Sciences of Dokuz Eylül University
In Partial Fulfillment of the Requirements for the Degree of Master of
Science in Environmental Engineering

by
Güneş KURŞUN

June, 2015
İZMİR

M.Sc THESIS EXAMINATION RESULT FORM

We have read the thesis entitled **"PRODUCTION AND APPLICATION OF PHOTOCATALYSTS FOR DETOXICIFATION OF CONTAMINATED WATER"** completed by **GÜNEŞ KURŞUN** under supervision of **PROF. DR. AYŞEGÜL PALA** and we certify that in our opinion it is fully adequate, in scope and in quality, as a thesis for the degree of Master of Science.
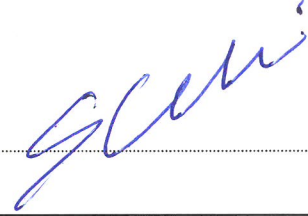
Prof. Dr. Ayşegül PALA

Supervisor

Prof. Dr. Delya SPONZA   Prof. Dr. Erdal ÇELİK

Prof.Dr. Ayşe OKUR

Director

Graduate School of Natural and Applied Sciences

ACKNOWLEDGMENTS

I would like to express my special thanks to my advisor Professor Dr. Ayşegül PALA, for useful remarks and engagement, willingly shared her precious time and experiences, continuous support throughout this study. It was pleasure to work with her.

I would like to thank to Prof. Dr. Erdal ÇELİK for his guidance, advices on experiments with his valuable support on metallurgical and material part of this study.

I would also like to thank all members of center of application and production of electronic materials (EMUM). I am also grateful to Asst. Prof. Dr. Mustafa EROL for his valuable helps in metallurgical and material steps of the thesis.

I also want to thank to my project partners Fatma BAKAL and Özlem CANPOLAT, my laboratory partners Ruti Ruth POLITI and Gülek ÖNER for their helps in experimental studies of the thesis and support.

I owe more than thanks to my family members and my girlfriend for their trust, motivation, encouragement and endless support.

Güneş KURŞUN

PRODUCTION AND APPLICATION OF PHOTOCATALYSTS FOR DETOXIFICATION OF CONTAMINATED WATER

ABSTRACT

The main objective of this study is to produce potassium lanthanium titanates (KLTO) photocatalysts on silicon substrates via sol-gel method by spin coating to photooxidize of cyanide and methylene-blue compounds in the water. Acute Toxicity test with Daphnia magna were performed to evaluate toxicity of methylene-blue (MB) and cyanide. Different thermal analysis - Thermogravimetry (DTA-TG), Fourier Transform Infrared (FTIR), X-Ray Diffraction (XRD) and Scanning Electron Microscope (SEM) analyses were carried out to see phase identification and surface morphology of the KLTO, respectively. Photocatalytic degredation tests were investigated in a Suntest CPS solar simulator. The measurement of an absorbance values were carried out with the help of Schmadzu UV-mini 1240 spectrometer. Batch- reactor was designed and produced for application and testing of thin films.

KLTO thin films were successfully coated on silicon substrates. Photocatalytic degredation tests, SUVA toxicity tests and Acute toxicity tests were investigated. It was found that KLTO thin films exhibited less toxic effect on Daphnia magna acute toxicity test of methylene blue azo-dye and cyanide. Photocatalytic degradation tests were more successful with KLTO thin films. With the prototype reactor, KLTO thin films were collected in a designed reactor and achieved maximum efficiency.

Keywords: Sol-gel technique, photocatalytic, KLTO, methylene blue, cyanide.

KİRLENMİŞ SULARIN DETOKSİFİKASYONUNDA FOTOKATALİZÖRLERİN ÜRETİMİ VE UYGULANMASI

ÖZ

Bu çalışmanın temel amacı, sularda siyanür ve metilen mavisi bileşiklerini fotookside etmek için, potasyum lantanyum titanat (KLTO) fotokatalizörlerin silikon altlıklar üzerine sol-jel yöntemiyle üretilmesidir. Siyanür ve metilen mavisi (MB) toksik etkisinin belirlenmesi için Daphnia magna akut toksisite testi gerçekleştirilmiştir. KLTO 'nun faz analizi ve yüzey morfolojisini görebilmek için Farklı termal analiz-termogravimetre (DTA-TG), Fourier dönüşümlü kızılötesi (FTIR), X ışınları difraktometresi (XRD) ve Taramalı elektron mikroskobu (SEM) analizleri sırasıyla gerçekleştirilmiştir. Fotokatalitik parçalanma testeri Suntest CPS solar simülatör cihazında gerçekleştirilmiştir. Absorbans değerlerinin ölçümünün Schimadzu UV-mini 1240 spektrofotometrenin yardımıyla gerçekleştirilmiştir. İnce filmlerin uygulaması ve test edilmesi için kesikli-reaktör dizayn edilip üretilmiştir.

KLTO ince filmleri başarılı bir şekilde silikon altlıklar üzerine kaplanmıştır. Fotokatalitik parçalanma testleri, SUVA toksisite testleri ve Akut toksisite testleri gerçekleştirilmiştir. KLTO ince filmler, metilen mavisinin Daphnia magna akut toksisite testinde daha az toksik etki sergilediği bulunmuştur. Fotokatalitik parçalanma testleri KLTO ince filmleri ile birlikte daha başarılı olmuştur. Prototip reaktör ile birlikte, KLTO ince filmleri tasarlanan reaktörde toplanmıştır ve maksimum verim elde edilmiştir.

Anahtar kelimeler: Sol - jel tekniği, fotokatalitik, KLTO, metilen mavisi, siyanür

CONTENTS

LIST OF FIGURES

Page

LIST OF TABLES

CHAPTER ONE
INTRODUCTION

Water plays an important role in human, animal life, and ecosystem, but any unwanted addition of chemical substances leads to contamination or pollution and makes it unfit for consumption. Lately, environmental pollution is becoming the world debating and challenging problem. Among all those problems, water pollution is of prime concern. Water pollution has become an important problem at the global level. Anthropogenic and industrial activities are responsible for this pollution. Effluents are discharged directly or indirectly by the industries into the nearby water resources without proper treatment (Ameta et al., 2013). With the rapid economic development, many countries are face with an increasing water crisis, due to the water scarcity and quality deterioration in recent years (Cao et al., 2009).

The degradation of dyes in industrial effluent has attracted great attention in the recent years because of increasing environmental awareness and the application of environmental rules. Howbeit, some treatments for color removal from these effluents do not guarantee the absence of other secondary toxic substances, often arising from the treatment process itself (Immich et al., 2009).

Textile industry effluents contain dyes which make the water colored and toxic and unfit for use. Conventional treatment methods are used for removing color from water. Riera-Torres et al. reported a coagulation–flocculation and nanofiltration methods for degradation of dye from water (Riera-Torres et al., 2010).

Dyeing activities occur problems due to discharging of effluents. If not treated properly, these effluents may cause critical concern if it reaches potable water resources. In addition, synthetic dyes need to be removed from wastewaters because some dyes, and their degradation products, can be toxic and affect photosynthesis due to the reduction of light penetration (Figueiredo et al., 2000).

Azo dyes which especially coming from textile wastewater, cause color and toxicity problem. Among all synthetic colorants groups azo dyes are the most important. They are determined as xenobiotic compounds. Recently it has been showed that several microorganisms are able, under certain environmental conditions, to transform azo dyes to colorless products (Stolz, 2001).

In recent years, photocatalytic specialized materials and devices are increased not only in academic case but also in industrial applications. This dramatic rise accompanies with the population growth and wastes which are increased by them. New technological improvements are invented continuously. Owing to the environmental pollution, these new approaches should be eco - friendly. In 1969, according to a Japan researcher called Fujishima, photocatalysts used for the treatment process. Honda - Fujishima realized a prototype: Fine powders which are doped with metal and/or metal oxide particles were used as a photocatalyst in chemical reactions. These fine powders were semiconductor. Photocatalytic reactions with using TiO_2 were discovered by them. Among these years many research have been done to improve the photocatalytic systems (Kodama & Suzuki, 2007).

According to recent literature studies, anions or transition metals can be doped to TiO_2 to increase photocatalytic activity. Within the improvements of TiO_2 new approaches are enhanced like perovskite type layered materials. It has been reported that perovskite types are more effective than TiO_2. Ion exchange occurs immediately with perovskite type layered structures in terms of the geometry. One of them is lanthanum– titanates ($K_2La_2Ti_3O_{10}$ - KLTO). $La_2Ti_3O_{10}$- octahedral perovskite layers and substitutional K ions constitute the structure. This structure provides hydration of toxic and persistent organic matters in aqua solutions with the presence of UV light; in this way it presents high photocatalytic activity (Takata et al., 1997).

Photocatalytic mineralization of methylene blue using TiO_2 coated polystyrene beads reported by (Fabiyi & Skelton , 2000). Dhananjeyan et al. observed the effect of dopants and calcination temperature on the photocatalytic reaction of TiO_2 with certain pyrimidine bases (Dhananjeyan et al., 2000). Surface modification effect of

TiO$_2$ with ascorbic acid on photocatalytic degradation of an azo dye has been studied by (Ou et al., 2005).

Ikeda et al., (1998) were studied preparation of K$_2$La$_2$Ti$_3$O$_{10}$ by polymerized complex method and photocatalytic decomposition of water. Cui et al., (2006) were produced layered perovskite K$_2$La$_2$TiO$_{10}$ by high temperature solid state sintering and characterized by XRD and UV-Vis DRS. Ni and Pt dopants were added to understand the effectiveness. Yang et al., (2009) were produced K$_2$La$_2$TiO$_{10}$ via sol-gel method and doped with Vanadium (V). V was increased the photocatalytic activity of K$_2$La$_2$TiO$_{10}$.

The purposes to focus on thesis;
- Production and application of K$_2$La$_2$Ti$_3$O$_{10}$ photocatalysts using sol-gel method,
- Photocatalytic degradation tests of K$_2$La$_2$Ti$_3$O$_{10}$ thin films,
- To evaluate acute toxicity and SUVA toxicity tests and
- Design and produce a photocatalytic reactor for application of K$_2$La$_2$Ti$_3$O$_{10}$ thin films

CHAPTER TWO
THEORETICAL BACKGROUND

2.1 Photocatalysis

In 1972, Fujishima and Honda discovered the photocatalytic splitting of water on TiO_2 electrodes (Fujisima & Honda, 1972). This event opened the beginning of a new era in photocatalysis. Since then, research efforts in enhancing the photocatalytic efficiency of TiO_2 have come from extensive research has been studied by chemists, physicists, and chemical engineers. Applications to environmental cleanup have been one of the most active areas in heterogeneous photocatalysis. This is inspired by the application of TiO_2-based photocatalysts for the total mineralization of organic compounds in contaminated air and wastewaters (Ollis et al., 1993).

Photocatalysis is commonly used to describe the process in which the acceleration of a reaction occurs when a material, generally a semiconductor, interacts with light of sufficient energy (or of a certain wavelength) to produce reactive oxidizing species (ROS) which can lead to the photocatalytic transformation of a pollutant. It must be noted that during the photocatalytic reaction, at least two events must occur simultaneously in order for the successful production of reactive oxidizing species to occur. Typically, the first involves the oxidation of dissociatively adsorbed H_2O by photogenerated holes, the second involves reduction of an electron acceptor by photoexcited electrons; these reactions lead to the production of a hydroxyl and superoxide radical anion, respectively (Mills & Hunte, 1997).

A catalyst is not changing during the reaction or being consumed or change the speed of reaction. Photo-catalysis is identified as "acceleration by the existence of catalyst". On another words, the same process of catalyst is occurred by the presence of sunlight and semiconductor. The difference between catalytic and photocatalytic systems are the activated zones (Ohtani, 2010).

In photocatalysis, light of energy greater than the band gap of the semiconductor, excites an electron from the valence band to the conduction band (Figure 2.1). In the case of anatase TiO_2, the band gap is 3.2 eV, therefore UV light ($\lambda \leq 387$ nm) is required. The absorption of a photon excites an electron to the conduction band (e-CB) generating a positive hole in the valence band (Pelaez et all, 2012).

$$TiO_2 + hv \rightarrow h + VB + e - CB \qquad (2.1)$$
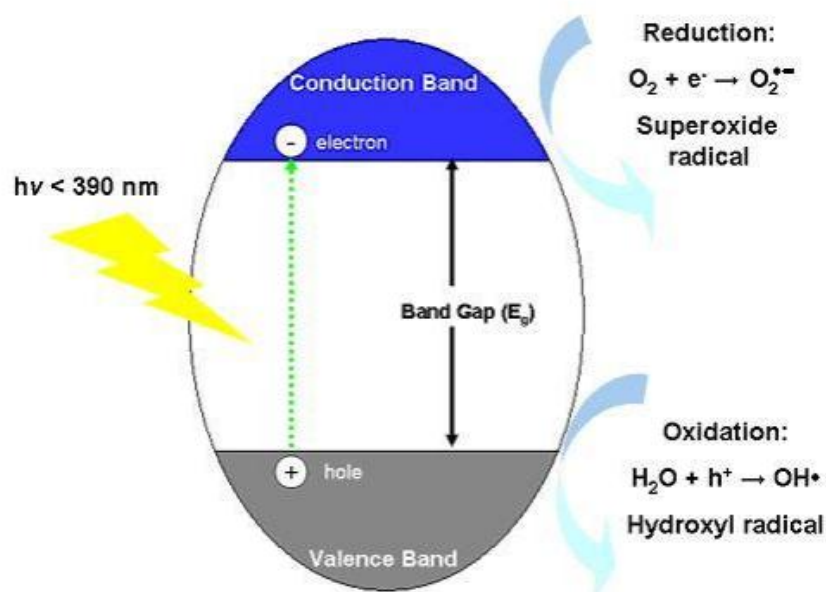
Figure 2.1 A schematic diagram of photocatalysis (Pelaez et al., 2012).

The light source needed for photosynthesis and photocatalyst. The light demonstrates the property of wave. Briefly, light has a wavelength and frequency. The formulas of $\lambda = c/\upsilon$ and $E = h.\upsilon$ help us to estimate the energy. In this formulation h is the Planck constant (6.63×10^{-34} J.s) and c is the velocity of light (3×10^8 m/s), υ is the frequency (1/s) and λ is the wavelength (nm). If the frequency is increased, the wavelength will be decreased and the energy will be increased. Different wavelengths have different energy level. That is why the photocatalytic activity is directly affected by the energy ($h.\upsilon$) of the ray and the efficiency increases (Nimetoğlu, 2011).

2.1.1 Photocatalytic Systems

The mechanism of photocatalysis is demostrated in Figure 2.2. After the absorption of light, some processes may occur such as electron-hole pair either recombines or migrates to the surface leading to oxidation and reduction of the adsorbates. Recombinations can occur at the surface or within the bulk of the photocatalyst (Bakal, 2014).
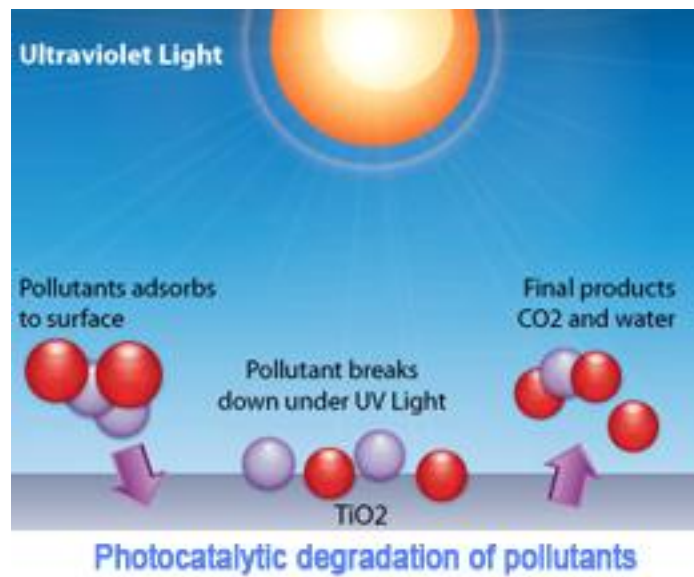
Figure 2.2 Photocatalytic degradation system (Environmental Science, 2015).

The semiconductor TiO_2 has been widely utilised as a photocatalyst for inducing a series of reductive and oxidative reactions on its surface. This is solely contributed by the distinct lone electron characteristic in its outer orbital. When photon energy (hv) of greater than or equal to the bandgap energy of TiO_2 is illuminated onto its surface, usually 3.2 eV (anatase) or 3.0 eV (rutile), the lone electron will be photoexcited to the empty conduction band in femtoseconds. Fig. 2.3 depicts the mechanism of the electron e hole pair formation when the TiO_2 particle is irradiated with adequate hv. The light wavelength for such photon energy usually corresponds to $l < 400$ nm. The photonic excitation leaves behind an empty unfilled valence band, and thus creating the electron-hole pair $(e^- - h^+)$ (Chong et al., 2010)
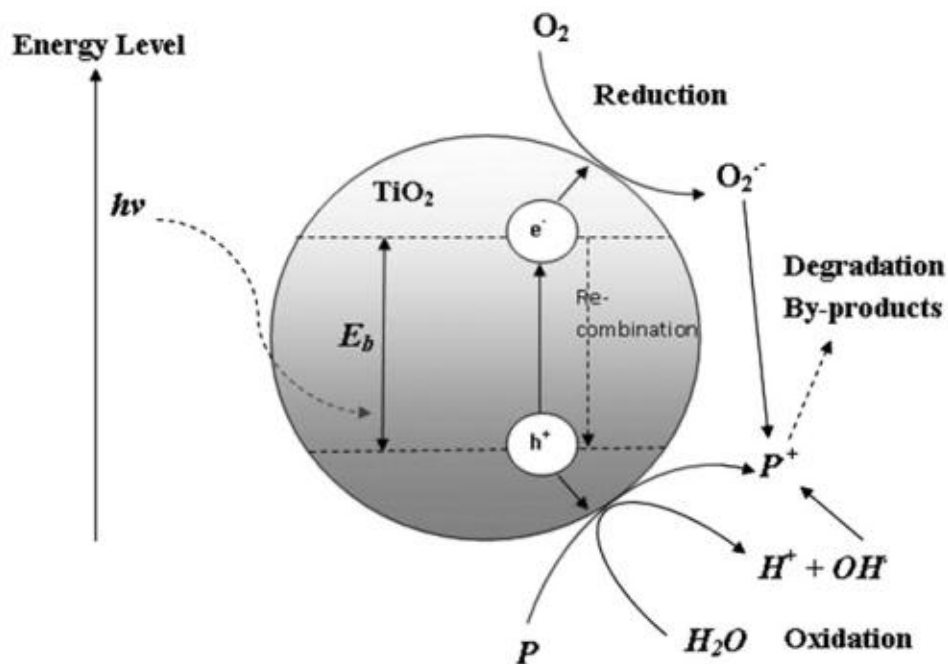
Figure 2.3 The mechanism of photocatalytic system. (Chong et al., 2010)

2.2 Semiconductors and Their Electrical Properties

Materials are collected on three category according to their electrical conductivity. These categories are classied as conductors, semiconductors and insulators.

The most popular of photocatalyst is titanium dioxide. Semiconductors can conduct due to the external effects of conductors. Normally, these materials are conductor and when heat, light, magnetic effect or electrical stress are applied, some electrons become independent and become conductor. If these external effects are removed, they return to their old type as insulator. This property provides a wide application on electronic area (Nimetoğlu, 2011).

A property of metals and semiconductors are separated from non - conductive insulators for one reason. The difference between them is because of the energy orbitals. Energy orbitals are very small. Due to this reason, electrons can be excited from lower energy levels to higher energy level. These small orbital energy

differences are called bands. Otherwise, these bands are so close together as energy that it takes so small amount of energy to support electrons to these higher band levels. The higher energy level that the valence electrons can be excited to is defined as the conduction band; because the electrons in this band are free to carry an electric current (Nimetoğlu, 2011). Conductor, insulator and semiconductor band energy levels are shown in Figure 2.4.

a)   b)   c)
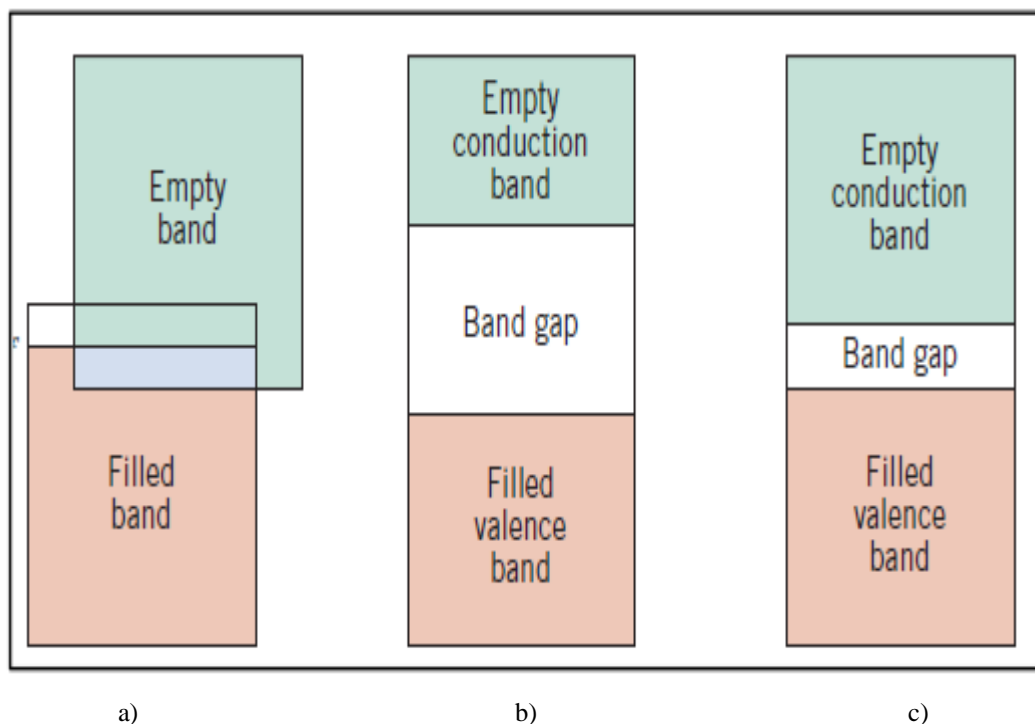
Figure 2.4 Conductor (a) , insulator (b) and semiconductor (c) band energy levels (Callister, 2008).

The semiconductor TiO_2 nanoparticles has been widely utilised as a photocatalyst for inducing a series of reductive and oxidative reactions on its surface. This is solely attributed to the distinct lone electron characteristic in its outer orbit. When photon energy (hv) of greater than or equal to the bandgap energy of TiO_2 is illuminated onto its surface, usually 3.2 eV (anatase) or 3.0 eV (rutile), the lone electron will be photo-excited to the empty conduction band in femtoseconds. The mechanism of the electron hole pair formation when the TiO_2 particle is irradiated with enough hv is illustrated in Figure 2.5 (Giwa et al., 2012).
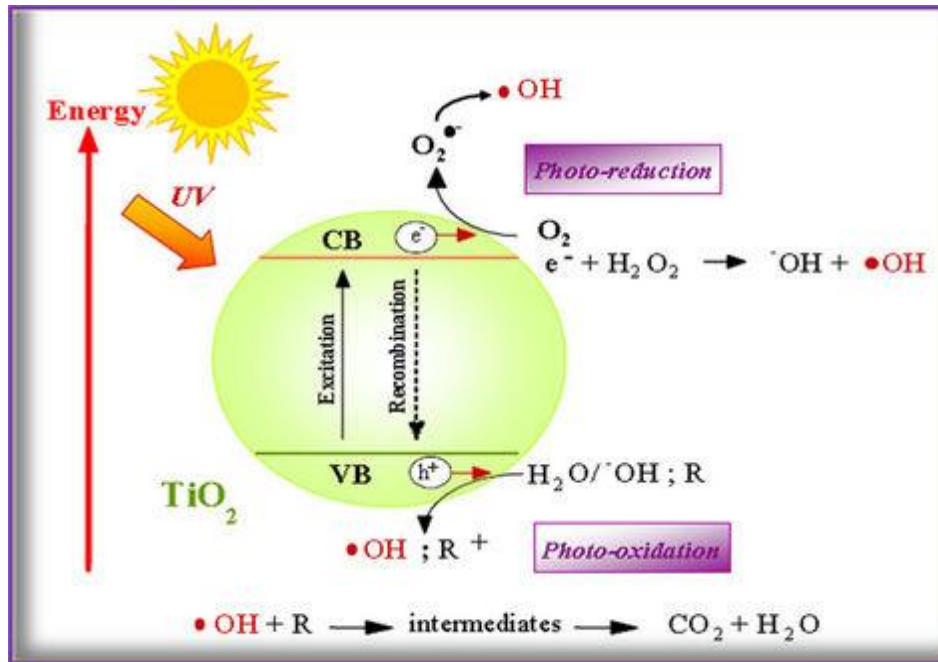
Figure 2.5 Semiconductor TiO_2 (Giwa et al., 2012).

2.3 Photocatalytic Degradation System

Boehm has estimated that the theoretical maximum surface coverage is 5-15 OH-/nm 2, depending on which crystal plane is being considered. Surface hydroxyl groups on TiO_2 illustrated in Figure 2.6.
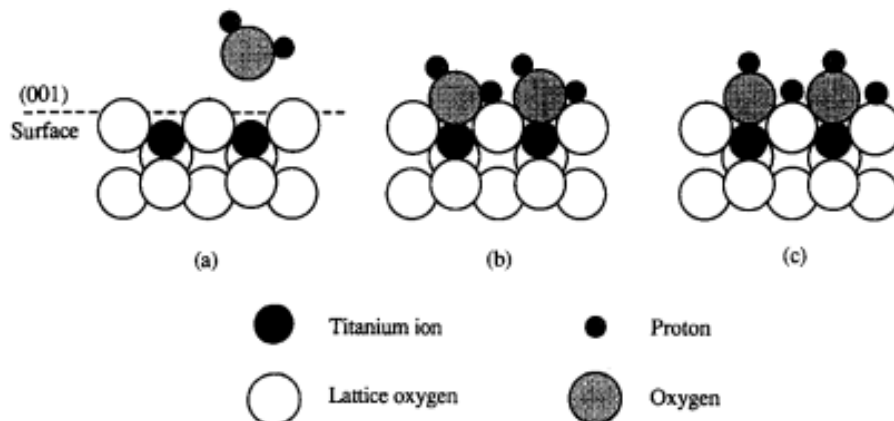
Figure 2.6 Surface hydroxyl groups on TiO_2. (a) Hydroxyl-free surface; (b) physical adsorption of water; (c) dissociation of water, giving rise to two distinct OH groups (Boehm and Hermann, 1967).

The reactions separate into three categories: First category occurs active electron pairs and (e-/h+) pairs occurred (Eq. 2.1) (Yiğit, 2008).

$$TiO_2 \ + hv \ \rightarrow e^-_{CB} \ + h^+_{VB} \tag{2.2}$$
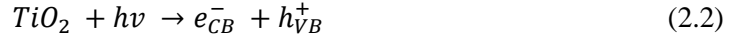
The combined h+ holes react with H_2O or OH^- ions and generate the activated •OH radical, and simultaneously the electrons are captured by Ti^{3+} and reacted with O_2 molecules to produce the oxygen anion radical. In the second stage includes oxidation of organic compounds to CO_2 and H_2O (Yiğit, 2008).

$$H_2O + h^+_{VB} \rightarrow OH\bullet + H^+_{(aq)} \tag{2.3}$$

$$e^-_{CB} + O_2 + H^+_{(aq)} \rightarrow OH\bullet + HO_2\bullet \tag{2.4}$$

$$e^-_{CB} + H_2O_2 + H^+_{(aq)} \rightarrow OH\bullet + H_2O \tag{2.5}$$

$$e^-_{CB} + O_2 \rightarrow O_2^-\bullet \tag{2.6}$$

$$2O_2^{--} + 2H^+_{(aq)} \rightarrow H_2O_2 + O_2 \tag{2.7}$$

$$e^-_{CB} + H_2O_2 \rightarrow OH\bullet + OH^-_{(aq)} \tag{2.8}$$

$$Cl_2C = CHCl + OH\bullet \rightarrow Cl_2C\bullet - CHCl - OH \tag{2.9}$$

$$Cl_2C\bullet - CHCl - OH + (O_2, H_2O_2) \rightarrow CO_2 + H_2O + HCl \tag{2.10}$$
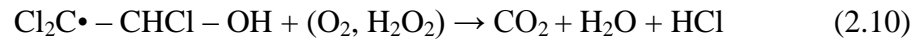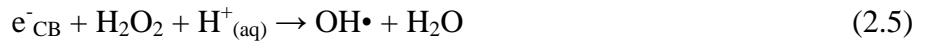
2.4 The Crystal Structure of $K_2la_2Ti_3O_{10}$

The structure of $K_2La_2Ti_3O_{10}$ has been confirmed as a layered perovskite-type compound and shown schematically in Figure 2.7. The $K_2La_2Ti_3O_{10}$ consists of negatively charge lanthanum titanate perovskite layer and interlayer K^+ ions . The adjacent triple perovskite sheets, $La_2Ti_3O_{10}$, are stacked with a displacement by 1/2 along the (001) direction. A lanthanum ion occupies the 12-fold site in the center of the perovskite lattice. According to the X-ray diffraction date, the parameters of $K_2La_2Ti_3O_{10}$ cell area=b=0.387 nm, c=2.98 nm, the face distance (001)=1.49 nm, and the thick of $La_2Ti_3O_{10}$ is 1.19 nm (Huang et al., 2010).

Literature researches on lanthan-titanates which is one of the layered structures increasing trend. With lanthan-titanates ($K_2La_2Ti_3O_{10}$) in perovskite structure are more active than TiO_2, this topic has been extensively investigated with a big interest (Yang et al., 2009).
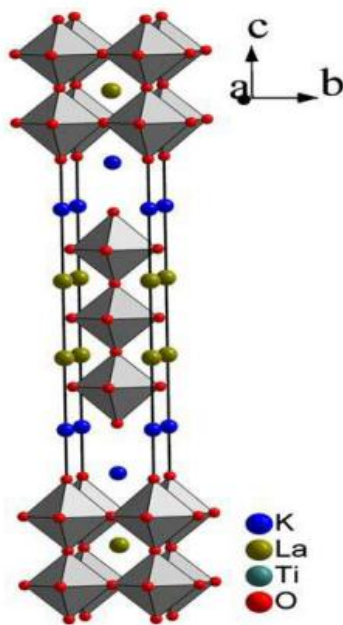
Figure 2.7 Schematic structure of KLTO (Huang et al., 2010)

2.5 Toxicity

Aquatic toxicology is the qualitative and quantitative study of the adverse or toxic effects of chemical substances or other anthropogenic and xenobiotic materials on aquatic organisms. The toxic effects include mortality as well as sublethal effects such as changes in growth, development, reproduction and behavior (Rand, 1995).

Daphnia magna is a microcrustacean which has been commonly used as a test organism in acute and chronic toxicity studies of several chemical compounds present in aquatic ecosystems. It is the most used species in the world for toxicity tests due to its sensitivity to toxic agents. This microcrustacean has a short cycle and reproduces by parthenogenesis, being easy to handle in the laboratory (United States Environmental Protection Agency [USEPA], 1985). Immich et al., (2009) reported removal of remazol red (RR) dye from aqueous solutions with Neem leaves and evaluation of their acute toxicity with Daphnia magna.

CHAPTER THREE
MATERIAL AND METHOD

3.1 The Purpose of the Thesis

The main aim of this study is to produce potassium lanthanum titanate $K_2La_2Ti_3O_{10}$ as a new generated nanotechnologic photocatalytic material by using sol-gel method. K, La and Ti based precursor materials, solvents, methanol, ethanol and glacial acetic acid chelating agent were prepared. To see the solution characterists, pH values, turbidity and rheological properties were measured from the prepared solutions. In order to provide clean substrates, silica substrates were cleaned inside on a methanol solution with Ultrasonic cleaner.

Thermogravimetry-Differential Thermal Analyzer (DTA – TG) and Fourier Transform Infrared (FTIR) tests were performed for xerogels. Thin films were coated with spin-coating method. The crystalline structure of $K_2La_2Ti_3O_{10}$ coated thin films was investigated at X-Ray Diffraction (XRD). Surface morphology and micro structure tests were performed by Scanning Electron Microscopy (SEM). Photocatalytical properties of the $K_2La_2Ti_3O_{10}$ coated thin films were evaluated using Schimadzu UV-mini 1240 (UV-Vis) spectrophotometer. Photocatalytic degradation, acute toxicity treatment tests, phenol and cyanide degradation tests were performed in ATLAS SUNTEST CPS+ solar simulator. This simulator provided Uv-light source between (300 nm $< \lambda <$800 nm). The light intensity can be changeable between 250-765 W/m^2. Acute toxicity tests were performed with *Daphnia Magna*. Photocatalytic reactor was designed and produced to achieve higher photocatalytic degradation rate and application of this study as a prototype.

3.2 Materials

KLTO thin films were produced by using Si (100) substrates. Precursors, solvent and chelating agent were demonstrated in Table 3.1. Lanthanum (III) 2,4 pentanedionate hydrate, potassium 2,4 pentanedionate hydrate, titanium (IV) isopropoxide, propionic acid, glacial acetic acid (GAA) was used chemicals to prepare thin films solution by using sol-gel method.

Table 3.1 Used precursors, solvent, chelating agent for preparing KLTO based thin films

Chemical Type	Chemical Name	Chemical Formula	Purity
Precursors	Lanthanum (III) 2,4 pentanedionate hydrate	$C_5H_{21}LaO_6.xH_2O$	-
	Potassium 2,4 pentanedionate hydrate	$C_5H_7KO_2.xH_2O$	97 %
	Titanium (IV) isopropoxide	$C_{12}H_{28}O_4Ti$	95 %
Solvent	Propionic acid	$C_3H_6O_2$	99 %
Chelating agent	Glacial acetic acid (GAA)	CH_3COOH	99.9 %

3.3 Production Process

Spin coating, dip coating and solution dropping methods are mostly used sol-gel based coating methods. Spin coating technique was used for this study. Spin coating is a procedure used to apply uniform thin films to flat substrates. In short, an excess amount of a solution is placed on the substrate, which is then rotated at high speed in order to spread the fluid by centrifugal force.

A machine used for spin coating is called a spin coater, or simply spinner. Rotation is continued while the fluid spins off the edges of the substrate, until the desired thickness of the film is achieved. The used solvent is usually volatile, and simultaneously evaporates. Therefore, the higher the angular speed of spinning, the thinner the film. The thickness of the film also depends on the concentration of the solution and the solvent (Bakal, 2014).

Firstly, the homogeneous solution of potassium lanthanum titanium oxide in stoichiometric ratios was heated to 60^oC with constant stirring until gel was formed. Glacial acetic acid (GAA) was added into the solution in order to form a gel as a chelating agent. The gel was dried at 200^oC for 9 hours to remove the moisture of gel. Finally, the dried gel was calcined at 500^oC for 30 minutes with a heating rate of $5^oC/min$ and at 850^oC for 3 hours with a heating rate of $5^oC/min$ in order to produce $K_2La_2Ti_3O_{10}$ powders.

The films of KLTO based solutions were deposited on substrates with Spin 150 model spin coater. Spin coating technique was shown in Figure 3.1. At first 5

seconds the spinner accelerates up to 500 rpm to spread the solution and remove the excess of solution. Between 40th second to 50th second, spinner turns in a speed at 3000 rpm. At this step of operation the deposited solution spreads related to the parameters of wettability, viscosity, pressure etc. Third step is the deceleration step here vaporizing of the volatiles and residual solutions were removed in 10 seconds. Spin coating parameters was shown in Table 3.2. Production process diagram was shown in Figure 3.2.

Table 3.2 Spin coating parameters

Step	Time (s)	Rotation speed (rpm)
1	5	100
2	10	500
3	15	3000
4 (Final)	10	0
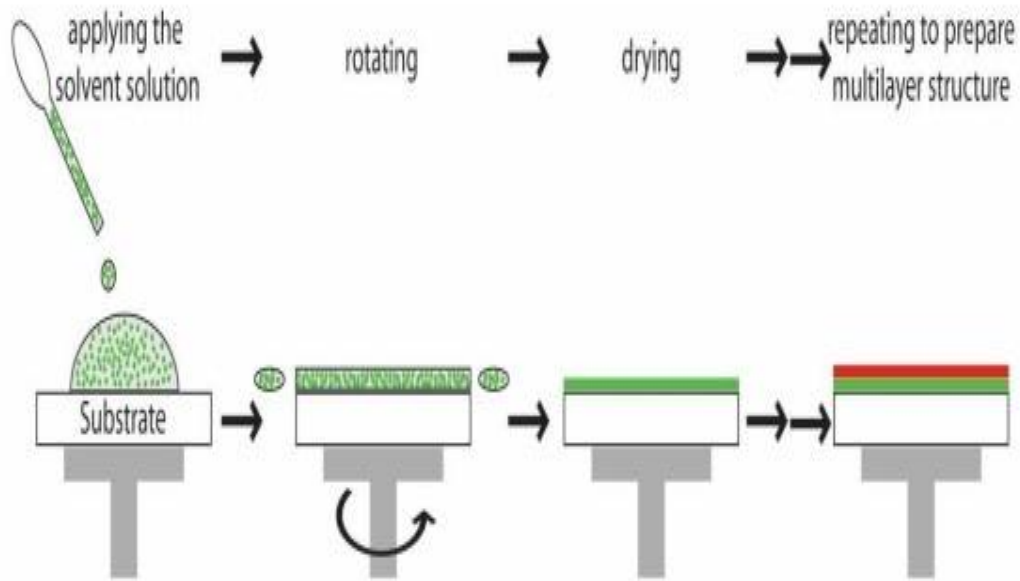
Figure 3.1 Spin coating technique (Anonym, n.d).

```
┌─────────────────────────┐   ┌─────────────────────────┐
│ Potassium 2,4 pentadionate│   │ Lanthanium 2,4 pentadionate│
│  hydrate dissolved in    │   │  hydrate dissolved in    │
│    propionic acid        │   │    propionic acid        │
│           ↓              │   │           ↓              │
│ Glaciel Acetic Acid (GAA)│   │ Titanium IV isopropoxide │
│       addition           │   │       addition           │
│           ↓              │   │           ↓              │
│ Homogeneous solution was │   │ Homogeneous solution was │
│       obtained           │   │       obtained           │
└─────────────────────────┘   └─────────────────────────┘
             │                            │
             ↓                            ↓
┌──────────────────────────────────────────────────────┐
│        Continious heating and stirring mixing          │
└──────────────────────────────────────────────────────┘
                          ↓
┌──────────────────────────────────────────────────────┐
│            Drying process at 200 °C, 9 h               │
└──────────────────────────────────────────────────────┘
                          ↓
┌──────────────────────────────────────────────────────┐
│             Calcined at 850 °C for 3h                  │
└──────────────────────────────────────────────────────┘
                          ↓
┌──────────────────────────────────────────────────────┐
│      KLTO powders was dispersed in propionic acid      │
└──────────────────────────────────────────────────────┘
                          ↓
┌──────────────────────────────────────────────────────┐
│            Coating on Si (100) substrates              │
└──────────────────────────────────────────────────────┘
                          ↓
┌──────────────────────────────────────────────────────┐
│            Annealed at 1100 °C for 8 h                 │
└──────────────────────────────────────────────────────┘
```

Figure 3.2 A flow scheme for production process

3.4 Characterization Process

The characterization process, photocatalytic degradation tests and toxicity tests of samples were performed by using the optimum for each thin film as shown in Table 3.3.

Table 3.3 The types of optimum photocatalysts

Sample number	Photocatalyst name
1	$K_2La_{1.1}Nd_{0.9}Ti_3O_{10}$
2	$K_2La_{1.9}Gd_{0.1}Ti_3O_{10}$
3	$K_2La_{1.5}Sm_{0.5}Ti_3O_{10}$
4	$K_2La_{1.5}Dy_{0.5}Ti_3O_{10}$

3.4.1 Turbidity

Turbidity tests were performed with VELP TB1 Model Turbidity Meter. The measurement range is from 0 ntu to 1000 ntu. In order to calculate turbidity five measurements were performed and the arithmetic means were taken.

3.4.2 pH Values

Following to preparation of transparent solutions, pH values of the solutions were measured to determine their acidic and basic characteristics using a standard pH meter with Mettler Tolede electrode.

3.4.3 Rheological Properties

The rheological measurements were conducted using a Bohlin Instruments CVO 100 Rheometer with 2 o conic plate geometry 60 mm in diameter and 0.7 μm gap sizes between plates. The viscosity values of KLTO solutions were performed at constant 300 Hertz frequency and 25 ^{o}C single shear mode. The rheological properties of the KLTO solutions were comparatively studied to characterize their gelation behaviours.

3.4.4 Contact Angle Measurement

Contact angle measurements of the solutions were performed with Contact Angle Meter-CAM 100 (KSV Instruments Ltd., Finland). It is a compact CCD camera based instrument for measurement of contact angles (CA) of liquids on solids. Goniometry involves the observation of a sessile drop of test liquid on a solid substrate. The basic elements of a goniometer include a light source, sample stage, lens and image capture. Contact angle can be assessed directly by measuring the angle formed between the solid and the tangent to the drop surface.

3.5 Process Optimization

3.5.1 Differential Thermal Analysis/Thermogravimetry (DTA/TG) Analysis

In order to use suitable process regime and to find reaction type of intermediate temperature products, DTA/TG analyses were performed under O_2 flowing for the $K_2La_2Ti_3O_{10}$ xerogel by using Shimadzu DTG-60H Model DTA-TGA. In addition, a detailed information regarding as decomposition, weight loss and phase formation was obtained by means of the same machine. Prior to the measurements, solutions were firstly dried at room temperature and subsequently fired to in the gel structure at 300 ^{o}C for 120 minutes in air. Measurements were carried out from room temperature to 1200 ℃ heating rate of 10 ^{o}C/min. The solutions were dried at 500℃ in 2 hours and powder was produced. The prepared xerogels were heated between 25℃ and 1200℃ with a 10 ℃/min heat change and oxygen atmosphere. The prepared KLTO based powders were heated in specific velocities in the presence of oxygen to determine the endothermic and exothermic reactions.

3.5.2 Fourier Transform Infrared (FTIR)

FTIR analyze was investigated from room temperature to 1000 ^{o}C temperature to determine how bond structure change according to process optimization related to increased temperature. FTIR (Perkin Elmer) samples of KLTO were measured between 4000 ve 400 cm^{-1} wavelength range.

3.6 Film Characterization

3.6.1 XRD Analysis

X-ray diffraction (XRD) patterns of KLTO thin films were performed by using a Thermo-Scientific, ARL-K$_\alpha$ diffractometer with a CuK$_\alpha$ irradiation (wavelength, λ=0.15418 nm). Measurements were performed by applying voltage of 45 kV and current of 44 mA. Scans were made over the range 2θ=2–70º in increments of 2º.

3.6.2 SEM Analysis

The Scanning Electron Microscope (SEM) is a versatile electron microscope that images a sample by scanning it with a high-energy beam of electrons in a raster scan-pattern. SEM analysis was performed to investigate surface morphology and characteristics of KLTO coatings by using JEOL JSM-6060 (SEM).

3.6.3 X-ray Photoelectron Spectroscopy (XPS)

X-ray Photoelectron Spectroscopy (XPS), irradiates the sample surface with a soft (low energy) X-ray. This X-ray excites the electrons of the sample atoms and if their binding energy is lower than the X-ray energy, they will be emitted from the parent atom as a photoelectron. Only the photoelectrons at the extreme outer surface (10-100 Angstroms) can escape the sample surface, making this a surface analysis technique (How xps works, n.d)

X-ray photoelectron spectroscopy (XPS) is the simplest analytical method for determining the species present at solid surfaces. XPS is a method widely used for both academic and technological studies and has a proven record for problem solving X-ray photoelectron spectroscopy (XPS) is the in areas ranging from corrosion and oxidation to simplest analytical method for determining the catalysis and microelectronics (Seah et al., 2001).

Thermo Scientific K-Alpha XPS system was used for elemental analysis of the KLTO coatings. Photoemission of electrons was produced using a monochromatic Al K_α X-ray source (1486.6 eV) operated at 150 W. The photoelectrons were allowed to pass through a hemisphericalanalyzer operated in fixed retardation ratio mode at 11.75 eV of pass energy. This results in an energy resolution of ≤ 0.51 eV. All data were acquired with take-off angle α of the detected electrons ranging from 30° to 70°.

3.6.4 Surface Roughness - AFM Analysis

The atomic force microscopy (AFM), invented by Binning, Quate, and Gerber (Binning et al., 1986). In AFM, a sharp tip at the end of a cantilever is scanned over a surface. While scanning, surface features deflect the tip and thus the cantilever. By measuring the deflection of the cantilever, a topographic image of the surface can be obtained. With adequate sensitivity in the deflection sensor, the tip can reveal surface profiles with subnanometer resolution (Miller et al., 1996). Therefore, surface characteristics of the KLTO films has been performed by using atomic force microscopy (AFM).

3.7 Photocatalytic Degradation Tests

Photocatalytic degradation performance tests were carried out with Atlas Suntes Cps+ solar simulator under 250, 750 W/m^2 light intensity. According to XRD, SEM and material studies the best of doped films was chosen as shown in Table 3.3 above. The light intensity was changed from 250 to 750 to understand the effect of light intensity. The pH values were shifted from 3, 7 to 10. In order to avoid evaporation, the beaker was lid by glass cap. In addition, air-conditioner was kept at 17 degrees to avoid evaporation. Initial absorbance was determined as A_o, and absorbance value of different times was determined as A_i.

$$\%\text{Degradation rate} = (A_o - A_i)/A_o \times 100 \qquad (3.1)$$

3.7.1 Suntest CPS+ Solar Simulator

Atlas suntest CPS+ was used in photocatalytical degradation tests of photocatalytsts. This xenon test instrument is with 560 cm^2 of exposure area. It is equipped with a flat specimen tray. The front view of Atlas Suntest CPS + solar simulator was shown in Figure 3.3.

① Coolant air supply Xenon lamp and regulation of test chamber temperature
② Coolant air outlet Xenon lamp and regulation of test chamber temperature
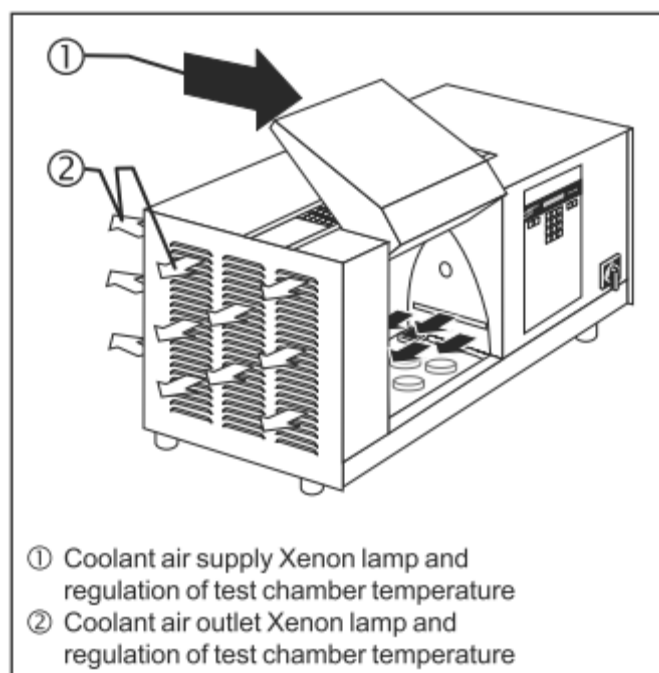
Figure 3.3 A view of Suntest Cps+ solar simulator (Atlas material testing, 1999).

3.7.2 Methylene Blue

Methylene blue is a heterocyclic aromatic chemical compound with the molecular formula $C_{16}H_{18}CIN_3S.3H_2O$. The papers, hair dye, fabric dying and wool dying industry has been widely used methylene blue as a colorant. Especially, the most methylene blue used industry is textile industry. It is commonly used in dyestuff applications and as a redox indicator. The mostly used wavelengths of MB are 291 and 664 nm. (Yao & Wang, 2010)
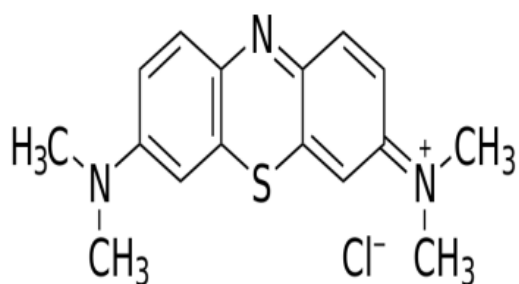
Figure 3.4 The chemical formula of MB (Yao & Wang, 2010)
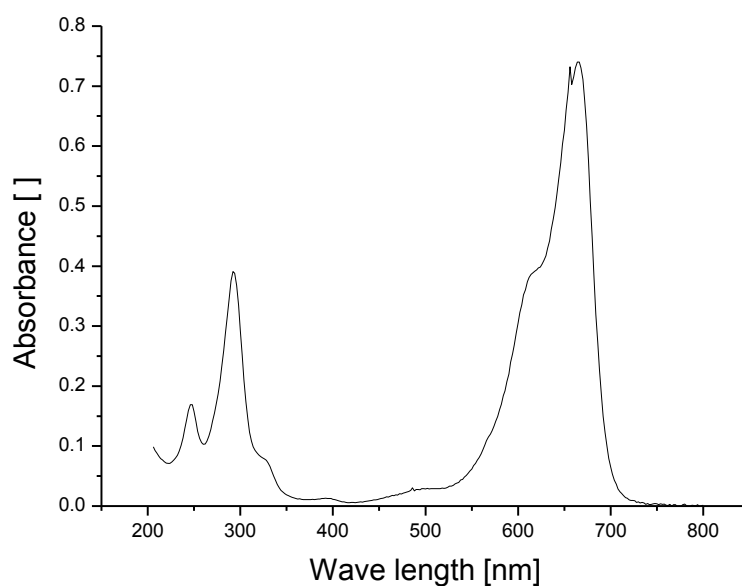
Figure 3.5 Degradation of 10^{-5} M methylene blue

3.7.3 Cyanide

Potassium cyanide (KCN) is mostly used in iron-steel and mine industry. Because of its properties and being common pollutant for industrial wastewaters, KCN was chosen for experiments. In this photocatalytical experiments potassium cyanide (KCN) was used as a solution. Potassium cyanide (KCN) was weighted as 65,12 g/mol and its density 1,52 g/cm^3 . Potassium cyanide KCN [151-50-8] is white crystalline solid. (Rubo et al., 2006). Physical properties of KCN are illustrated in Table 3.4.

Table 3.4 Physical properties of KCN (Rubo et al., 2006)

Physical quantity	KCN
M_r, relative molecular mass	65.119
Melting point	634.5 (98 wt %)
Density	1.553 g/cm^3 (20 ^{o} C)
	1.56 g/cm^3 (25 ^{o} C)
C_p, specific heat capacity	1.00 kj/kg/K
H, enthalpy (25 ^{o} C)	-112.63 kj/mol
H_f, heat of fusion	225 kJ/kg
Solubility in 100 g of ethanol, 100%,100 g of ethanol, 95%	0.57 g (19.5 ^{o} C)
Solubility in 100 g of methanol	4.91 g (19.5 ^{o} C)

3.8 Toxicity Tests

3.8.1 Acute Toxicity Tests

The acute toxicity of water was performed with treated methylene blue solution samples by using 24 h newborn *Daphnia magna* at different dilution rates. Acute toxicity experiments were investigated with 10 *Daphnids* for each beaker with 25 ml of effective volume. *Daphnia magna*'s were grown for 16 hours of daylight and 8 hours dark ambient. Room temperature was kept at 20± 2 ^{o} C, and after 24 hours of reaction time, immobility of *Daphnia magna*'s was calculated to determine EC_{50}.The acute toxicity test were performed with MB and KCN solution to determine toxic effects of MB dyes and KCN.

3.8.2 SUVA Toxicity Tests

SUVA toxicity test was performed at 254 nm wavelength. Wavelength measurements were carried out with Schimadzu UV-Vis mini 1240 spectrophotometer. $SUVA_{254}$ toxicity test was performed with the photocatalyst which was reached the best efficiency on treatment tests. To evaluate toxicity control (without photocatalyst) sample was placed. The effect of photocatalyst and pH to toxicity was investigated within SUVA toxicity tests. Equations (3.1) and (3.2) were used to evaluate SUVA toxicity.

$$SUVA = \frac{UVA}{DOC} * 100 \; cm/m \tag{3.2}$$

$$UVA = \frac{A}{d} \tag{3.3}$$

In which, A: Absorbance value at 254 nm and d: Length of cuvette.

3.9 Dissolved Organic Carbon (DOC) Test

Dissolved Organic Carbon (DOC) is the concentration of carbon remaining a water sample after the filtration of all particulate carbon and inorganic carbon. For DOC tests, the most effective photocatalyst $K_2La_2Sm_{0.5}Ti_3O_{10}$ in each photocatalyst set were sent to the laboratory to do analysis for 100 ml of wastewater. DOC was analyzed to determine SUVA.

CHAPTER FOUR
RESULTS AND DISCUSSION

4.1 Solution Characterists

4.1.1 Turbidity

The solution turbidity values are demonstrated in Table 4.1. Eventually, it is found that the prepared solutions were transparent and homogenous. it is important basis for further thin film applications, photocatalytic degradation and achieving best phase in KLTO materials using XRD. It was found that, the brown color coming from potassium powders increased turbidity value of KLTO thin films. If there are suspended particles in a liquid, the light will be scattered, and this results in a higher ntu value (Wilde & Gibs, 1998).

Table 4.1 Turbidity value of KLTO

Solution	Turbidity (ntu) *
KLTO	14.32

* The arithmetic mean of the value

4.1.2 pH Values

To estimate the solutions pH's, 5 measurements was done for each solution and their arithmetic mean was calculated. The arithmetic means of the pH values K, La, Ti - based solution was found to be 3.51. It was found that the solutions were showed acidic characteristic, due to the fact that this acidic condition is presence of the solvent and chelating agent.

4.1.3 Rheological Properties

Viscosity is the important factor to analyze the film thickness. Viscosity is an internal property of a fluid that offers resistance to flow. The angular velocity is found 300 Hz, the ambient temperature is 25°C, the time is determined 2500 s and 300 Hertz as test parameters for solutions viscosity. To investigate the gelling temperature with respect to different temperature, modulus of elasticity and viscous were measured. Figure 4.1 illustrates viscosity- time graphs.
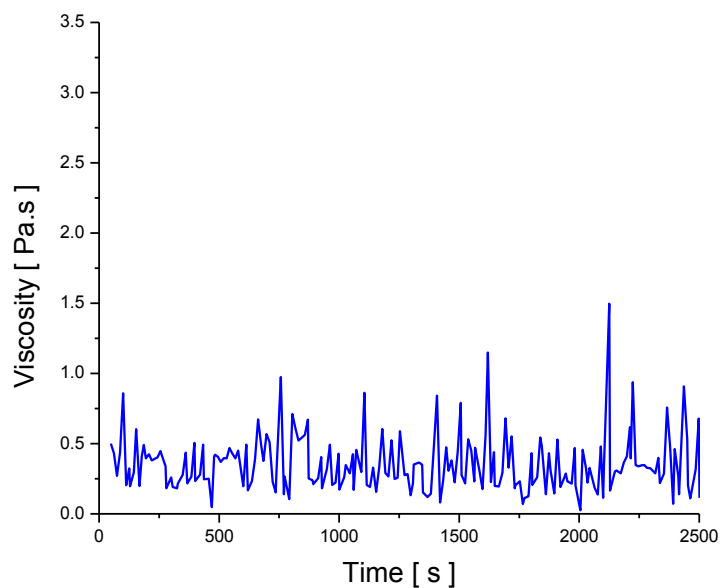
Figure 4.1 Viscosity versus time characteristic of $K_2La_{1.1}Nd_{0.9}Ti_3O_{10}$ solution

4.1.4 Contact Angle Measurement

Measurements showed that the contact angle values of K, La, Ti - based solutions are in the range of 4° and 3°. Inasmuch as the results are less than 90°, there is no inconsistency about wettability between substrates and solution.

4.2 Process Optimization

In order to produce material and to obtain optimum thermal heat condition these tests are performed. DTA – TG and FTIR analysis were carried out for this reason.

4.2.1 Differential Thermal Analysis/Thermogravimetry (DTA/TG) Analysis

Figure 4.2 shows the KLTO xerogel thermal behavior at 300°C and 120 minutes in air. Due to the change of heat treatment regime, endothermic and exothermic reactions occur. The first peak showed solvent removal at 200-210°C. The second peak showed carbon based materials coming from chelating agent, alkoxide and solvents completely burned out at 310°C.
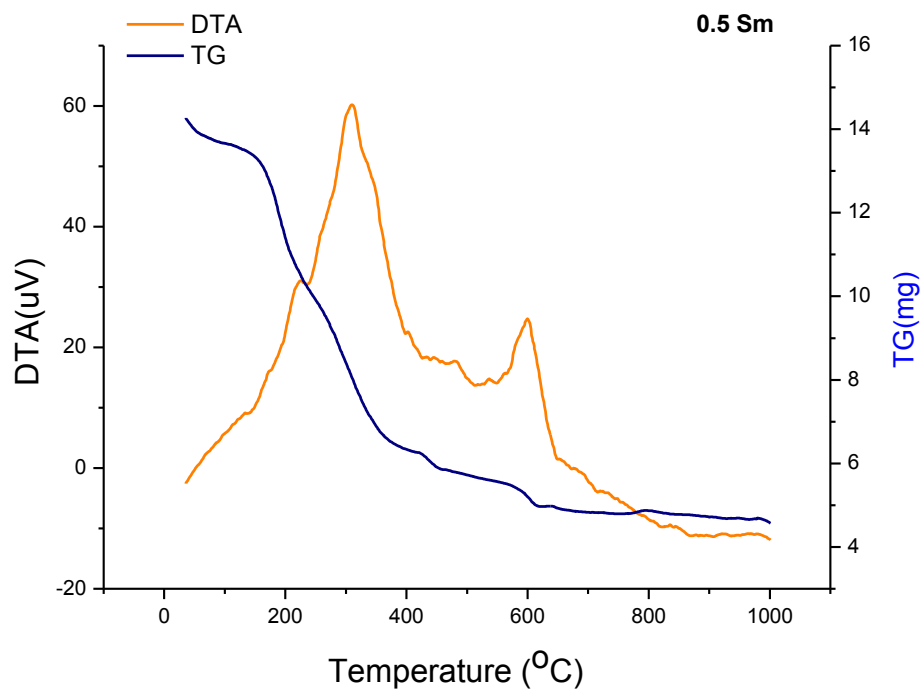
Figure 4.2 DTA/TG curve of 0.5 Sm doped KLTO xerogel

4.2.2 Fourier Transform Infrared (FTIR)

The absorbance spectrum of specimens was found at 25 ^{o}C and between the wavelengths 600-4000 cm^{-1}. Figure 4.3 gives information about the Sm doped KLTO spectra at specified temperatures such as 25, 50, 100, 200, 300, 400, 600, 800 and 1000°C for 15 minutes in air. O-H, C=O and M-OCOO-M bond frequencies are decreased and vanished around 600 °C. At 600 °C, any signal of O-H, C=O and M-OCOO-M bonds could not be found. As a result of these signals, organic structures and hydroxyls are completely vanished.
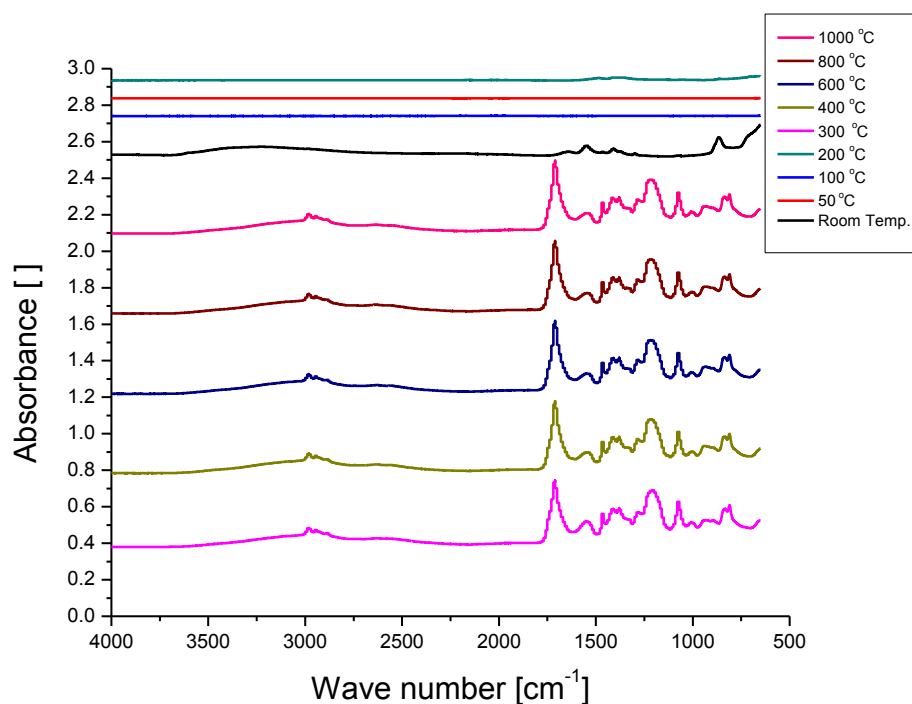
Figure 4.3 FTIR spectra of the Sm doped KLTO annealed at different temperatures

4.3 Film Characterization

4.3.1 XRD Analysis

Figures 4.4-4.7 illustrate the phase structures of KLTO films doped with Gd, Sm, Nd and Dy. As expected, the diffraction peaks were intense and sharp, indicating that the obtained $K_2La_2Ti_3O_{10}$ and $KLa_2Ti_3O_{9,5}$ were well crystallized. Note that the KLTO based coatings easily crystallized on Si (100) wafer as a perovskite phase after annealing process at 1100ºC for 8 hours.
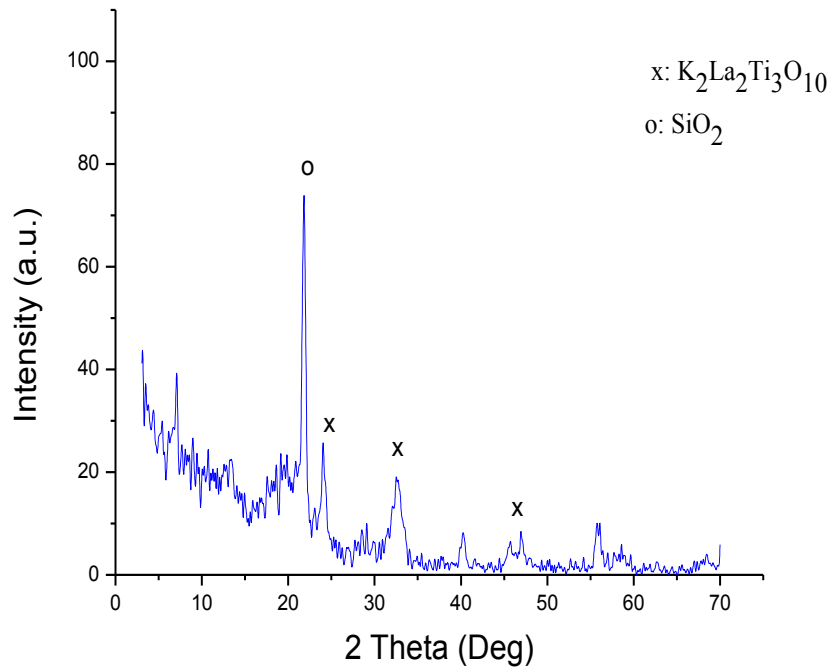
Figure 4.4 XRD pattern of $K_2La_{1.1}Nd_{0.9}Ti_3O_{10}$ films on Si substrate
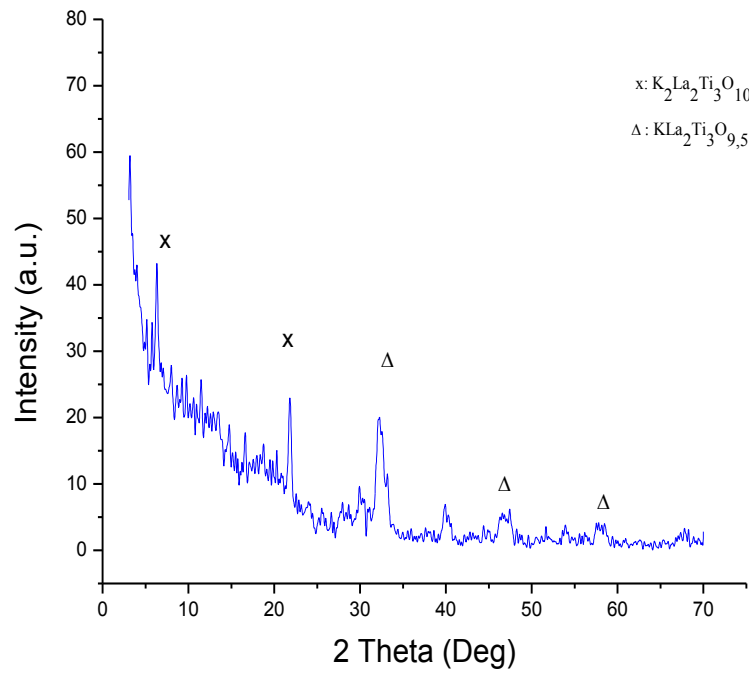
Figure 4.5 XRD pattern of $K_2La_{1.5}Sm_{0.5}Ti_3O_{10}$ films on Si substrate
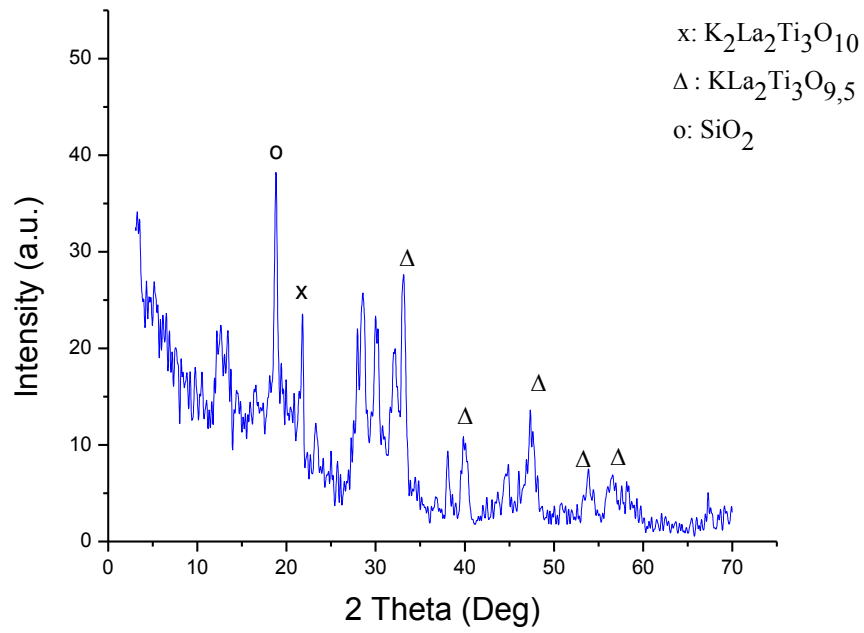
Figure 4.6 XRD pattern of $K_2La_{1.5}Dy_{0.5}Ti_3O_{10}$ films on Si substrate
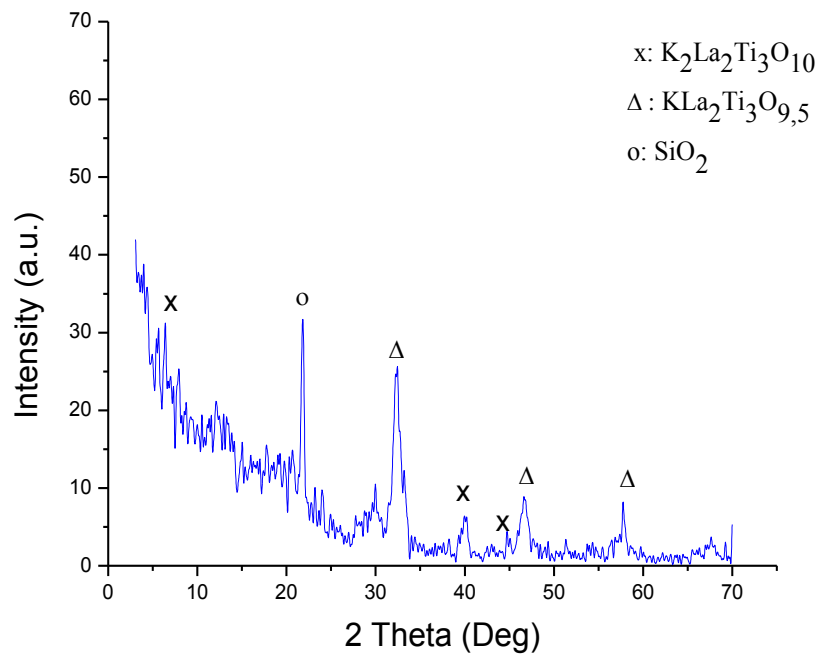
Figure 4.7 XRD pattern of $K_2La_{1.9}Gd_{0.1}Ti_3O_{10}$ films on Si substrate

29

4.3.2 SEM Analysis

The surface topography and morphology of coatings on Si (100) substrates were investigated by using JEOL JSM – 6060 (SEM) Scanning Electron Microscope.
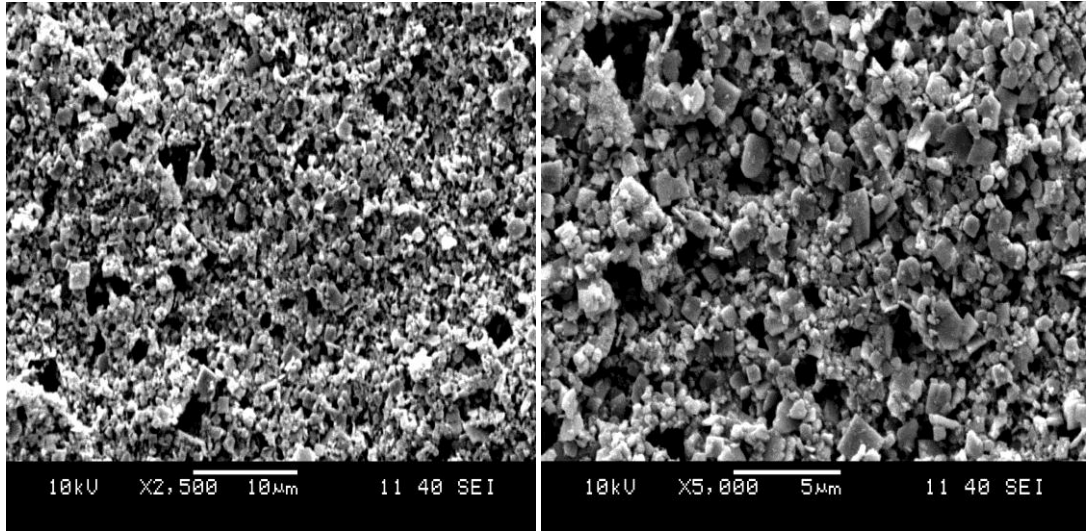
(a)
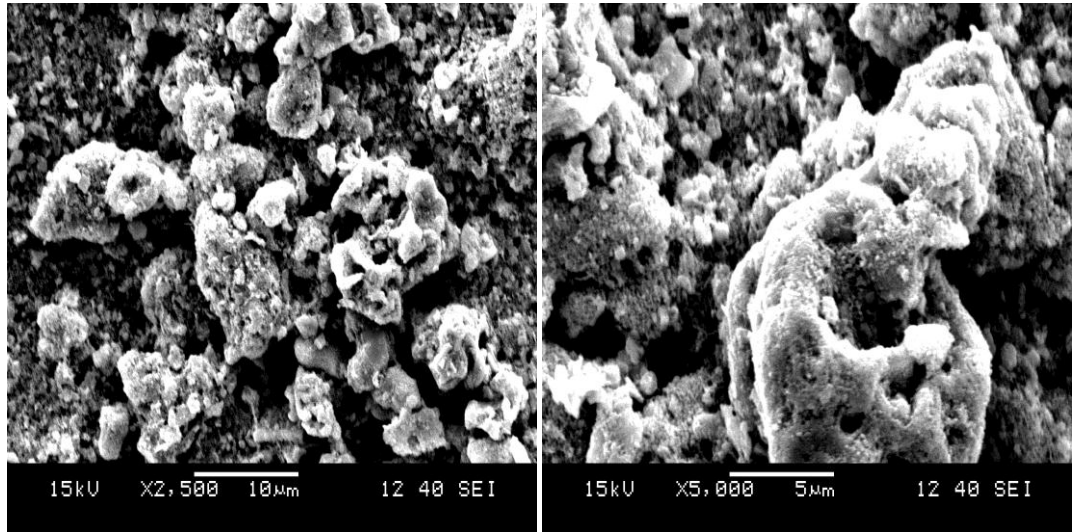
(b)

Figure 4.8. SEM micrographs of (a) $K_2La_{1.1}Nd_{0.9}Ti_3O_{10}$, (b) $K_2La_{1.9}Gd_{0.1}Ti_3O_{10}$, (c) $K_2La_{1.5}Sm_{0.5}Ti_3O_{10}$ and (d) $K_2La_{1.5}Dy_{0.5}Ti_3O_{10}$ coatings on Si substrates.
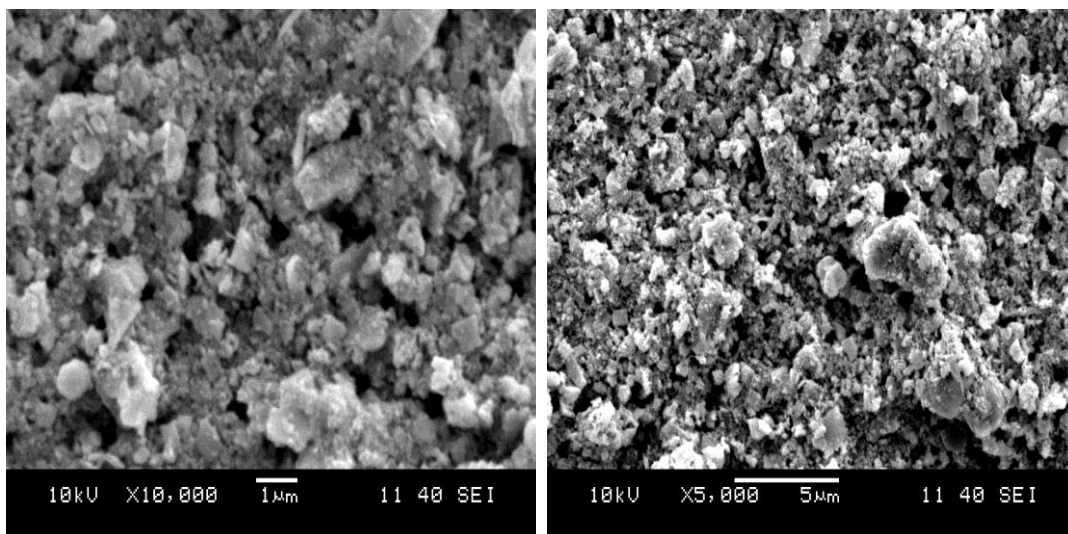
(c)
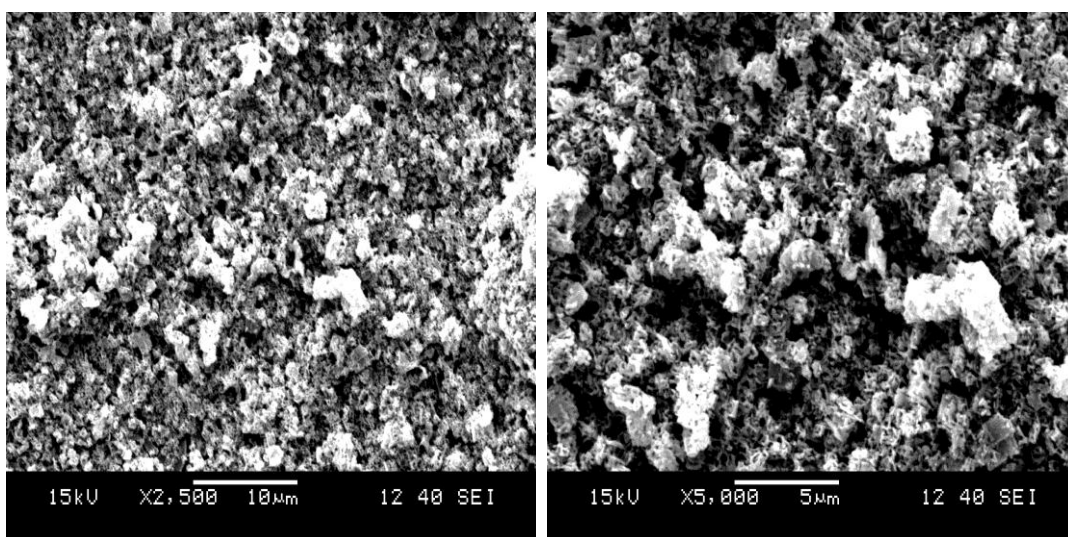
(d)

Figure 4.8. SEM micrographs of (a) $K_2La_{1.1}Nd_{0.9}Ti_3O_{10}$, (b) $K_2La_{1.9}Gd_{0.1}Ti_3O_{10}$, (c) $K_2La_{1.5}Sm_{0.5}Ti_3O_{10}$ and (d) $K_2La_{1.5}Dy_{0.5}Ti_3O_{10}$ coatings on Si substrates (continue).

The surface morphologies of KLTO films are shown in Figure 4.8. The morphology of the films is an important parameter that affects photocatalytical properties. The morphology of the KLTO coatings was found to be affected by solution concentration, pH, viscosity, film thickness, coating technique, and heat treatment regime. Spin coating method was performed with a spin-coater. Although spin coating is a technique which provides smooth surfaces, heat treatment regime resulted in this structure.. KLTO thin films are chosen to use for photocatalytical applications. According to literature, the surface area is important parameter for

acting with pollution and the photocatalytic efficiency is increased when the surface area is increased (Bakuy, 2009).

4.3.3 Elemental Analysis

Figure 4.9 shows XPS analysis of $K_2La_{1.1}Nd_{0.9}Ti_3O_{10}$, $K_2La_{1.9}Gd_{0.1}Ti_3O_{10}$, $K_2La_{1.5}Sm_{0.5}Ti_3O_{10}$ and $K_2La_{1.5}Dy_{0.5}Ti_3O_{10}$ thin films on Si wafer. According to the results, K, La, Ti, O elements, substrate material (Si) was obtained. In addition, dopant effects can be seen from Figure 4.9 showing Nd, Gd, Sm and Dy in the films.

a) b)

c) d)
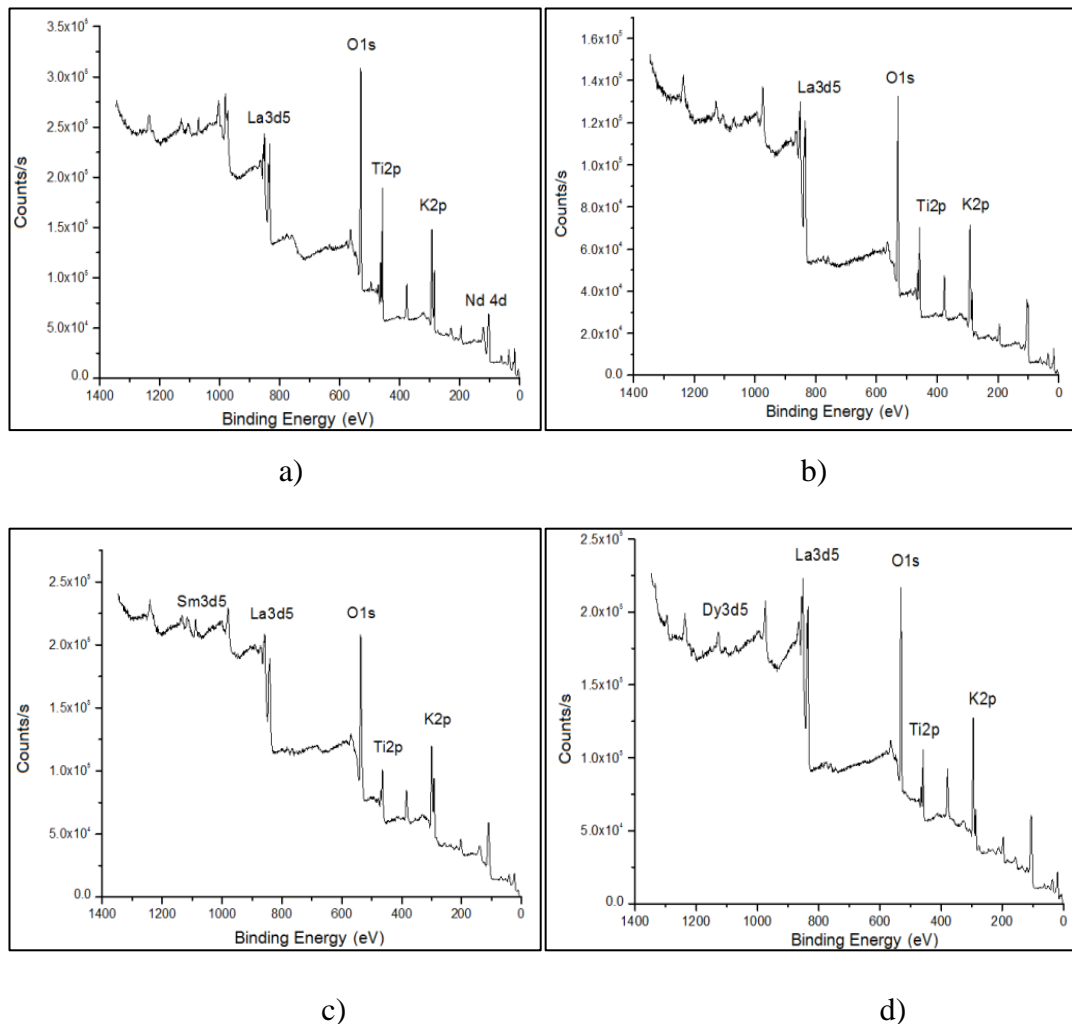
Figure 4.9 XPS analysis of (a) $K_2La_{1.1}Nd_{0.9}Ti_3O_{10}$, (b) $K_2La_{1.9}Gd_{0.1}Ti_3O_{10}$, (c) $K_2La_{1.5}Sm_{0.5}Ti_3O_{10}$ and (d) $K_2La_{1.5}Dy_{0.5}Ti_3O_{10}$ thin films.

4.3.4 Surface Roughness - AFM Analysis

The surfaces are granular. The average roughness of the 2 specimens was found 445.69 and 900.27 nm, respectively. The increasing change of roughness leads to good photocatalyst.
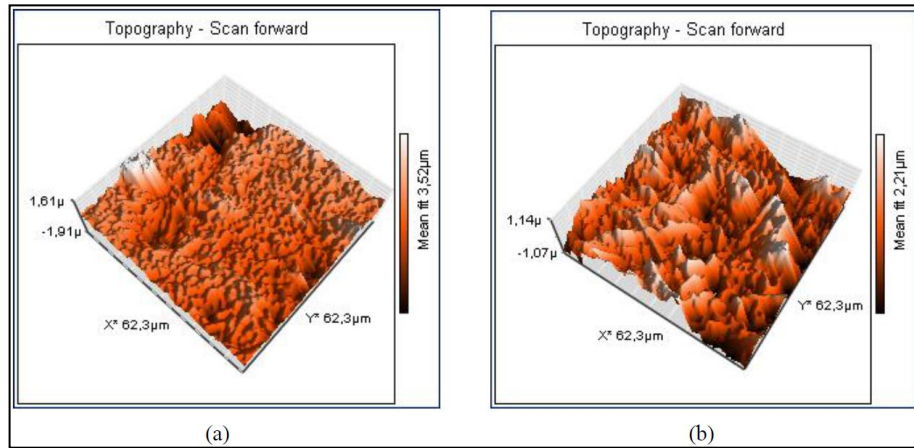
Figure 4.10 Atomic force microscope (AFM) scans of KLTO thin films

4.4 Photocatalytic Experiments

Completely degradation of MB was determined as optimum factor. As soon as photocatalytic degradation finish, MB solution samples were collected and spectrophotometer measurements were performed. Average time of degradation was found to be change with light intensity, time and pH. The best photocatalyts was found Sm doped KLTO (sample 3) according to photocatalytic experiments.

4.4.1 Photocatalytic Degradation Experiments under 250W/m^2 Light Intensity and pH=3

Photocatalytic degradation results pH=3 and 250W/m^2 light intensity was given in Figure 4.11. Degradation percentage of samples was shown in Table 4.2. Control sample was showed 20% degradation efficiency in contrast sample 3 was showed 86% degradation efficiency obtained in absence of KLTO.
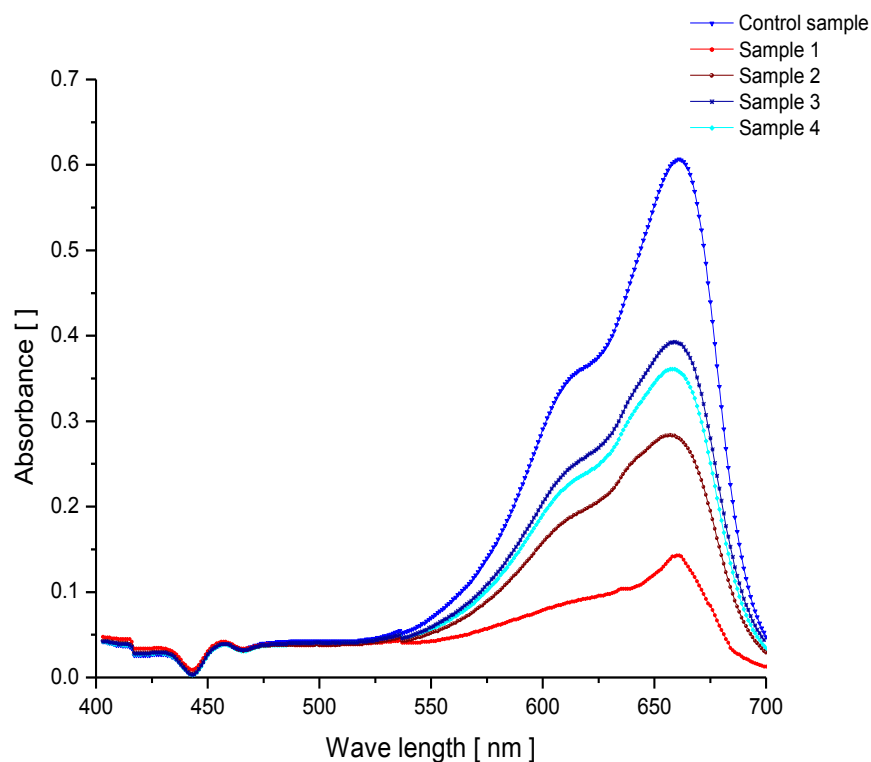
Figure 4.11 Methylene blue degradation absorbance vs. time after 5 hours (Co = 10^{-5} M, 250 W/m^2 and pH = 3)

Table 4.2 Degradation results under 250W/m^2 light intensity and 5 hours of reaction time

Sample Code**	Degradation efficiency*
1	53%
2	48%
3	86%
4	64%
Control	20%

*Degradation efficiency calculation was performed by using (3.1) equation.
**Explanation of sample codes were given in Table 3.3

4.4.2 Photocatalytic Degradation Experiments under 750W/m² Light Intensity and pH=3

90% degradation efficiency was reached in sample 3 as shown in Figure 4.12 and Table 4.3. In contrast to photocatalysts, control sample was showed 53% degradation efficiency.

Figure 4.12 Methylene blue degradation absorbance vs. time after 5 hours (Co = 10^{-5} M, 750 W/m² and pH = 3)

Table 4.3 Degradation results under 750W/m² light intensity and 5 hour reaction time

Sample Code**	Degradation efficiency*
1	59%
2	68%
3	90%
4	69%
Control	53%

*Degradation efficiency calculation was performed by using (3.1) equation.
**Explanation of sample codes was given in Table 3.3

4.4.3 Photocatalytic Degradation Experiments under pH=7 and 250W/m² Light Intensity

Photocatalytic degradation results of pH=3 and 250W/m² light intensity was shown in Figure 4.13. Degradation efficiencies of these samples was given in Table 4.4.

Figure 4.13 Methylene blue degradation absorbance vs. time after 3 hours (Co = 10^{-5} M, 250 W/m² and pH = 7)

Table 4.4 Degradation results under 250W/m² light intensity and 3 hours of reaction time

Sample Code**	Degradation Efficiency*
1	83%
2	90%
3	95%
4	87%
Control	68%

*Degradation efficiency calculation was performed by using (3.1) equation.
**Explanation of sample codes was given in Table 3.3.

As shown in Table 4.4 and Figure 4.13 control sample was performed 68% degradation rate and sample 3 was showed 95% degradation rate.

4.4.4 Photocatalytic Degradation Experiments under pH=7 and 750W/m² Light Intensity

Figure 4.14 illustrates degradation results under 750 W/m² light intensity at Suntest CPS+ and 3 hours of reaction time. Degradation percentage of samples was given in Table 4.5. The best photocatalyst was determined as Sample 3 according to experiment results with showing 97% degradation rate.

Figure 4.14 Methylene blue degradation absorbance vs. time after 3 hours (Co = 10⁻⁵ M, 750 W/m² and pH = 7)

Table 4.5 Degradation results under 750W/m^2 light intensity and 3 hours of reaction time

Sample Code**	Degradation efficiency*
1	71%
2	89%
3	97%
4	87%
Control	71%

Degradation efficiency calculation was performed by using (3.1) equation.
Explanation of sample codes was given in Table 3.3.

4.4.5 Photocatalytic Degradation Experiments under pH=10 and 250 W/m^2 Light Intensity

Methylene blue solution was completely degraded in a 30 minutes time under 250W/m^2 and pH=10. According to experiments, reaction time keep at 30 minutes. Spectrophotometer results were illustrated in Figure 4.15 and Table 4.6. Sample 3 showed 91% degradation efficiency respect to the control sample showed 59% photocatalytic degradation efficiency. Although it was found that 91 % degradation efficiency, it is possible to make photocatalyst more effective using different dopant elements (Yang et al., 2009).
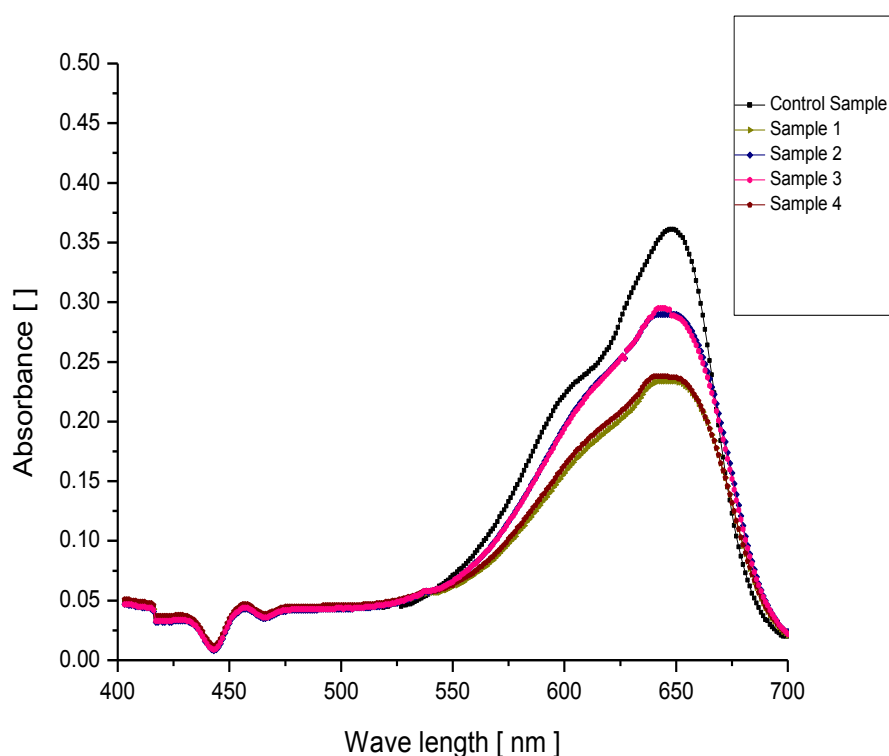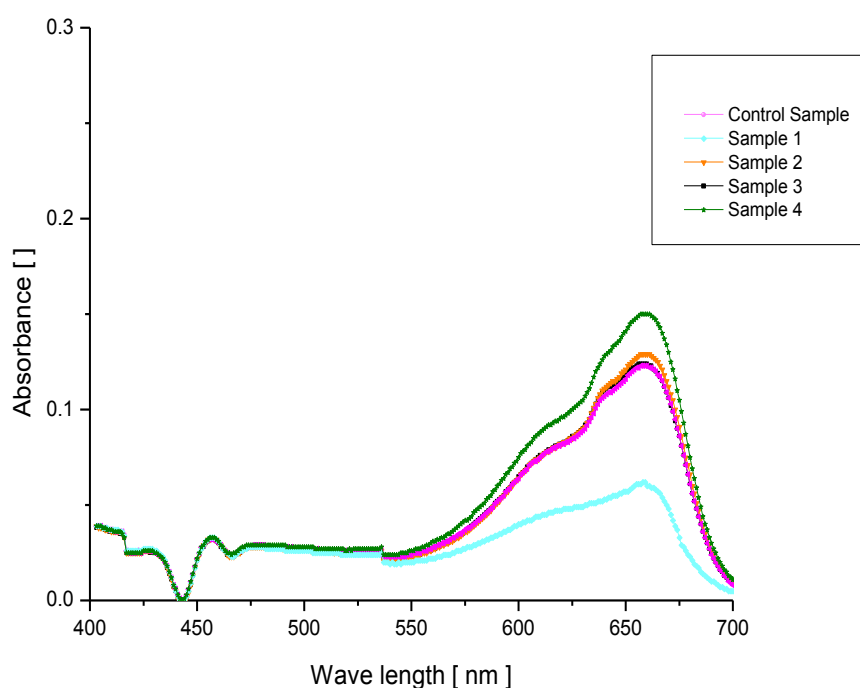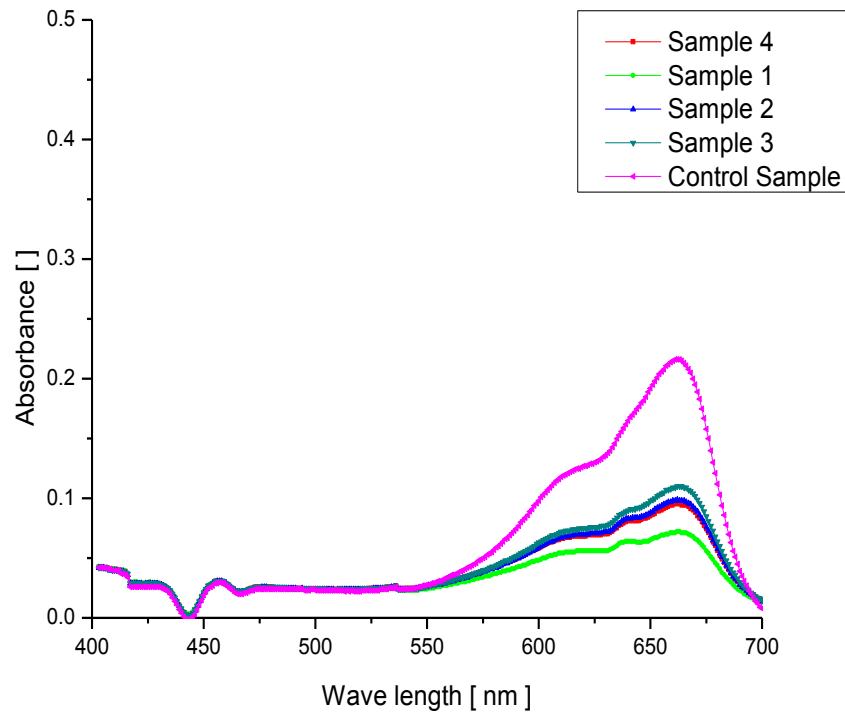
Figure 4.15 Methylene blue degradation absorbance vs. time after 30 minutes (Co = 10^{-5} M, 250W/m^2 and pH = 10)

Table 4.6 Degradation results under 250W/m^2 light intensity and 30 minutes time

Sample Code**	Degradation efficiency*
1	86%
2	85%
3	91%
4	87%
Control	59%

*Degradation efficiency calculation was performed by using (3.1) equation.
**Explanation of sample codes was given in Table 3.3.

4.4.6 Photocatalytic Degradation Experiments under pH=10 and 750 W/m^2 Light Intensity

Spectrophotometer result was illustrated in Figure 4.16 and Table 4.7. The best pH was found to be 10 according to experiments. 100% degradation efficiency was reached in 10-minute time.
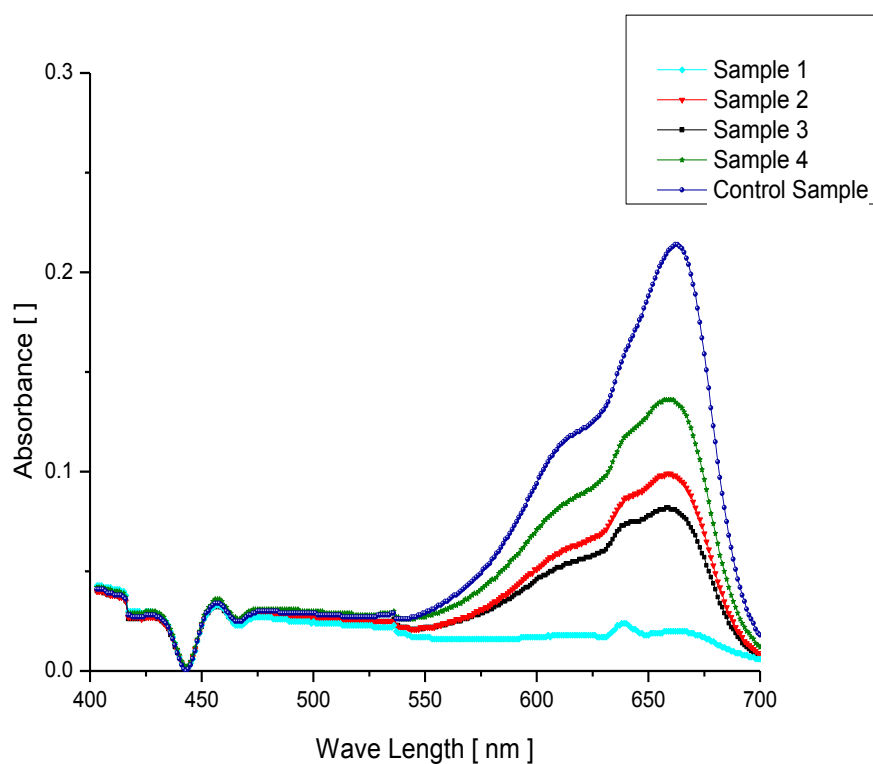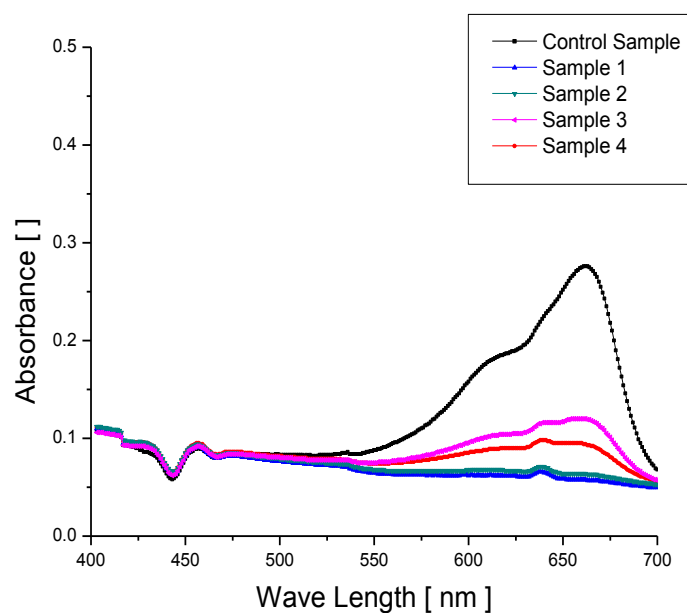
Figure 4.16 Methylene blue degradation absorbance vs. time after 10 minutes (Co = 10^{-5} M, 750W/m^2 and pH = 10)

Table 4.7 Degradation results under 750W/m^2 light intensity and 10 minutes time

Sample Code**	Degradation efficiency*
1	83%
2	82%
3	93%
4	76%
Control	64%

*Degradation efficiency calculation was performed by using (3.1) equation.
**Explanation of sample codes was given in Table 3.3.

4.5 DOC Results

The best effective photocatalyst, $K_2La_2Sm_{0.5}Ti_3O_{10}$ was chosen. Table 4.8 illustrated the results at pH of 7. 23.47% of mineralization was performed.

Table 4.8 DOC Results of blank sample and KLTO

Photocatalyst	DOC(mg/l)
Initial DOC	7.37
DOC after degradation with KLTO	5.64

4.6 SUVA Toxicity Tests

To evaluate Spesific UV Absorbance (SUVA) equation 3.3 was used. Sample 3 was chosen as the best photocatalyst and used in SUVA toxicity tests according to its high degradation efficiency. Results are shown in Tables 4.9-4.10 and Figure 4.17

Table 4.9 Absorbance values at 254 nm wavelength

Sample code	254 nm absorbance
Sample 3	0.129
Control (without photocatalyst)	0.408

Calculation was made by using (3.2) and (3.3) equation.

Table 4.10 SUVA$_{254}$ value of samples

Sample code	Suva$_{254}$ value*
Sample 3	2.29 L/mgM
Control (without photocatalyst)	5.53 L/mgM

Calculation was made by using (3.2) and (3.3) equation.
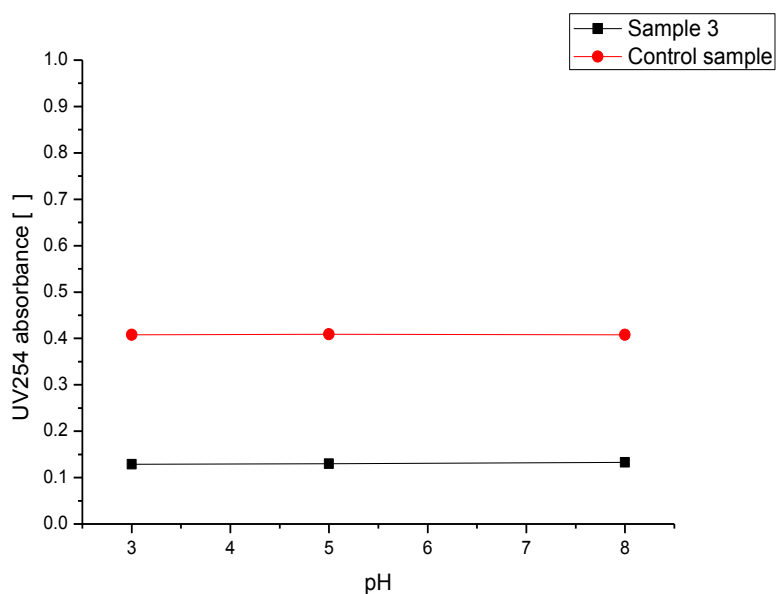
Figure 4.17 UV$_{254}$ Absorbance compared to pH values

4.7 Acute Toxicity Tests

4.7.1 Acute Toxicity Tests of Methylene Blue

Acute toxicity tests of MB were performed with four different samples and blank sample in this study. Immobility rate was calculated on the total number of *Daphnia magna* in a 24 hour period. The immobility percentage of MB was demonstrated on Tables 4.11-4.15. Regression line graphs of methylene blue with KLTO based coatings and blank sample can be seen in Figures 4.18-4.22.

Table 4.11 Immobility rates of *Daphnia magna'*s in MB solutions treated with sample 1

Concentration of solutions treated with sample 1 (%)	The number of active *Daphnia magna*	Immobility (Mortality) rate (%)
100	2	80
50	4	60
20	5	50
5	7	30

Table 4.12 Immobility rates of *Daphnia magna'* s in MB solutions treated with sample 2

Concentration of solutions treated with sample 2 (%)	The number of active *Daphnia magna*	Immobility (Mortality) rate (%)
100	3	70
50	4	60
20	5	50
5	6	40

Table 4.13 Immobility rates of *Daphnia magna'* s in MB solutions treated with sample 3

Concentration of solutions treated with sample 3 (%)	The number of active *Daphnia magna*	Immobility (Mortality) rate (%)
100	6	40
50	7	30
20	9	10
5	10	0

Table 4.14 Immobility rates of *Daphnia magna'* s in MB solutions treated with sample 4

Concentration of solutions treated with sample 4 (%)	The number of active *Daphnia magna*	Immobility (Mortality) rate (%)
100	2	80
50	4	60
20	5	50
5	7	30

Table 4.15 Immobility rates of *Daphnia magna'* s in methylene blue solutions treated with blank sample

Concentrations of blank sample (%)	The number of active *Daphnia magna*	Immobility (Mortality) rate (%)
100	0	100
50	2	80
20	4	60
5	5	50

Solutions were prepared at 5, 20, 50, 100 percentage dilution rates for treated water with sample 1 .In order to find EC_{50}, lethal concentration was calculated with crossing immobility percentage 50% and concentration. According to Figure 4.18 median effective concentration of sample 1 was found to be EC_{50}= 44%.

Immich et al., (2009) reported that if the color in dye not treated good, this result to an expressive mortality of *Daphnia Magna*'s in Remazol blue RR dye acute toxicity test. Similar to this study, methylene blue acute toxicity tests showed less toxicity with photocatalysts. Because photocatalysts performed good efficiency in photocatalytic degradation test.
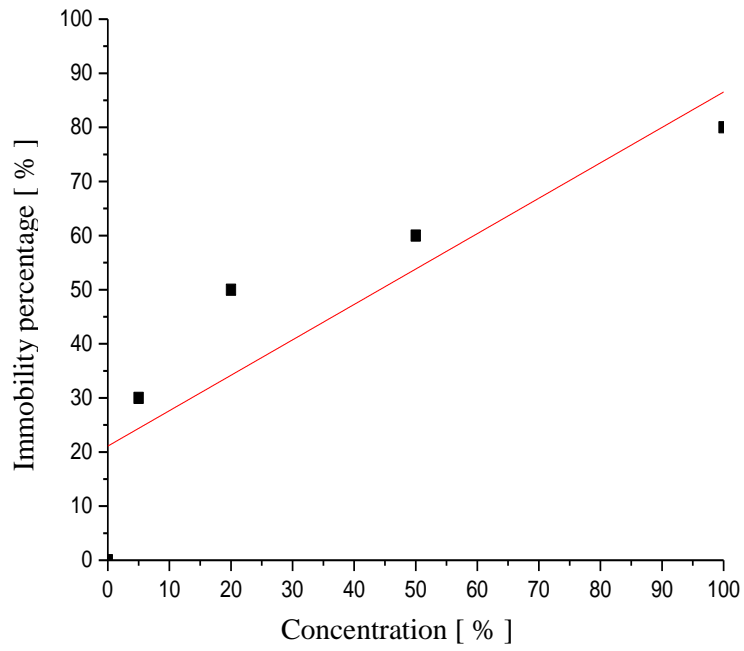
Figure 4.18 Concentration vs. immobility diagram of sample 1
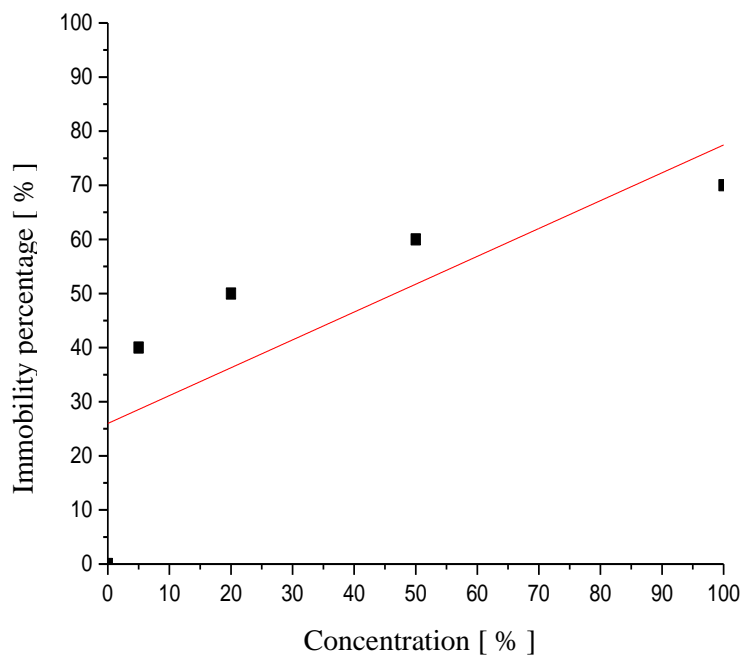
Figure 4.19 Concentration vs. immobility diagram of sample 2
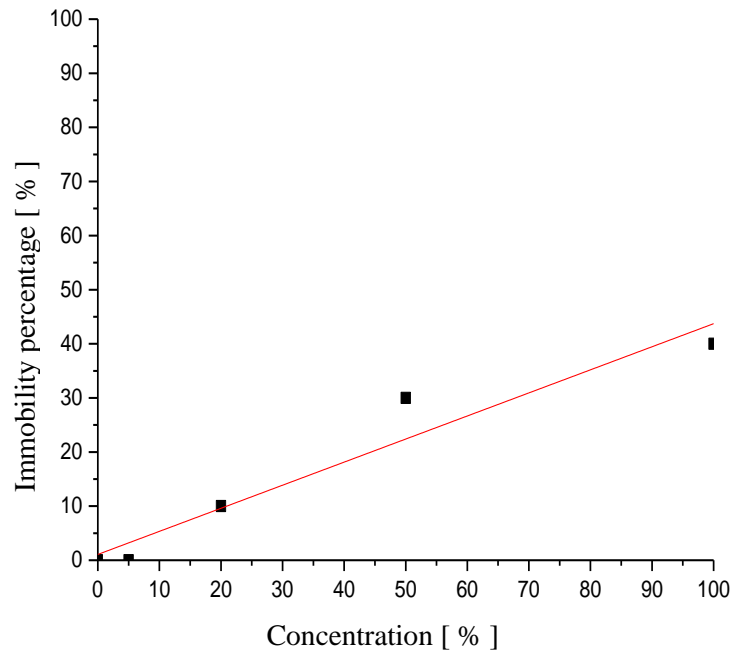
Figure 4.20 Concentration vs. immobility diagram of sample 3
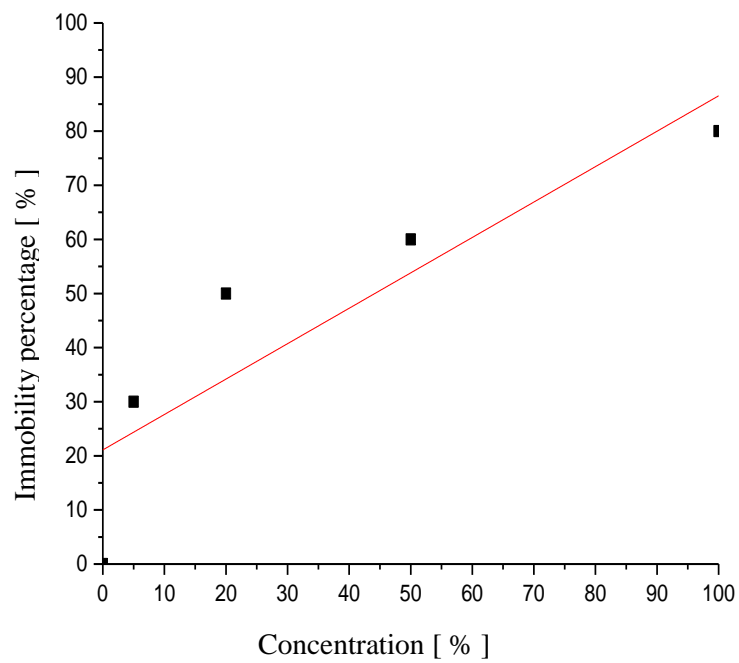
Figure 4.21 Concentration vs. immobility diagram of sample 4
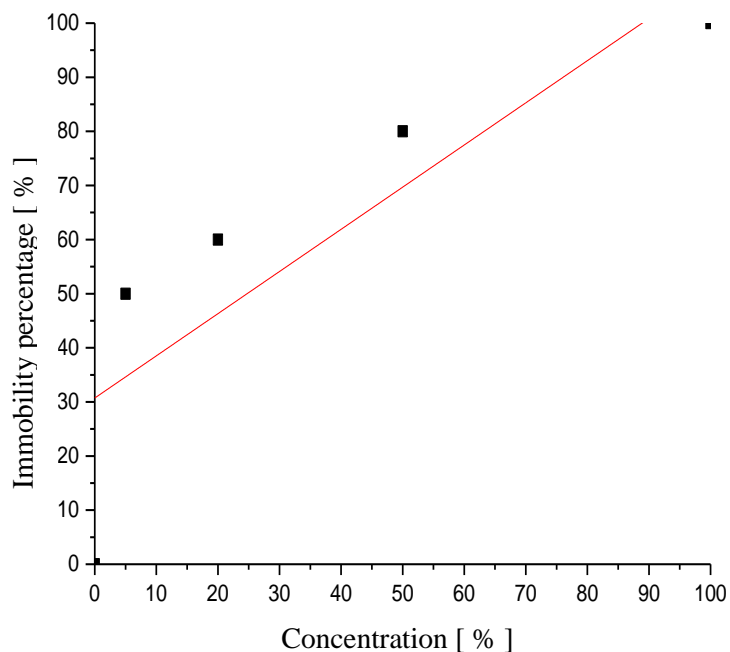
Figure 4.22 Concentration vs. immobility diagram of blank sample

The solutions were prepared at 5, 20, 50, 100 percentage dilution rates for treated water with sample 2 and median effective concentration was found to be $EC_{50}= 47$ % (Figure 4.19).

The solutions were prepared at 5, 20, 50, 100 percentage dilution rates for treated water with sample 3 and median effective concentration was found to be more than 100% (Figure 4.20).

The solutions were prepared at 5, 20, 50, 100 percentage dilution rates for treated water with sample 4 and median effective concentration was found to be 45 % (Figure 4.21).

The solutions were prepared at 5, 20, 50, 100 percentage dilution rates for treated water with blank sample and median effective concentration was found to be 23% (Figure 4.22)

EC$_{50}$ values were obtained for comparison of toxicity among these samples. EC$_{50}$ values of sample 1, 2, 4, 5 were found to be 44%, 47%, 45% and 23%, respectively. Highest rate of EC$_{50}$ were observed in sample 3. It is seen that EC$_{50}$ value of sample 3 was obtained more than 100 %. Highest treatment effect of KLTO was reached with sample 3. This led to more photocatalytical degradation and less toxicity. The best photocatalyst can be chosen as Sm doped KLTO which can be seen in sample 3. In contrast to these samples with KLTO photocatalysts, blank sample showed 23% of EC$_{50}$ value for acute toxicity of methylene blue. The samples having KLTO based coatings significantly more successful than blank sample for degradation and toxicity of methylene blue.

4.7.2 Acute Toxicity Tests of Potassium Cyanide [KCN]

Immobility rate was calculated on the total number of *Daphnia magna* in a 24 hour period. The immobility percentage of KCN was demonstrated in Tables 4.16-4.20. Immobilization versus concentration figures were shown in Figures 4.23-4.27.

Table 4.16 Immobility rates of *Daphnia magna'*s in KCN solutions treated with sample 1

Concentration of solutions treated with sample 1 (%)	The number of active *Daphnia magna*	Immobility (Mortality) rate (%)
100	1	90
50	3	70
20	4	60
5	5	50

Table 4.17 Immobility rates of *Daphnia magna'*s in KCN solutions treated with sample 2

Concentration of solutions treated with sample 2 (%)	The number of active *Daphnia magna*	Immobility (Mortality) rate (%)
100	1	90
50	2	80
20	3	70
5	5	50

Table 4.18 Immobility rates of *Daphnia magna*'s in KCN solutions treated with sample 3

Concentration of solutions treated with sample 3 (%)	The number of active *Daphnia magna*	Immobility (Mortality) rate (%)
100	4	60
50	6	40
20	7	30
5	9	10

Table 4.19 Immobility rates of *Daphnia magna*'s in KCN solutions treated with sample 4

Concentration of solutions treated with sample 4 (%)	The number of active *Daphnia magna*	Immobility (Mortality) rate (%)
100	2	80
50	3	70
20	4	60
5	6	40

Table 4.20 Immobility rates of *Daphnia magna*'s in KCN solutions treated with blank sample

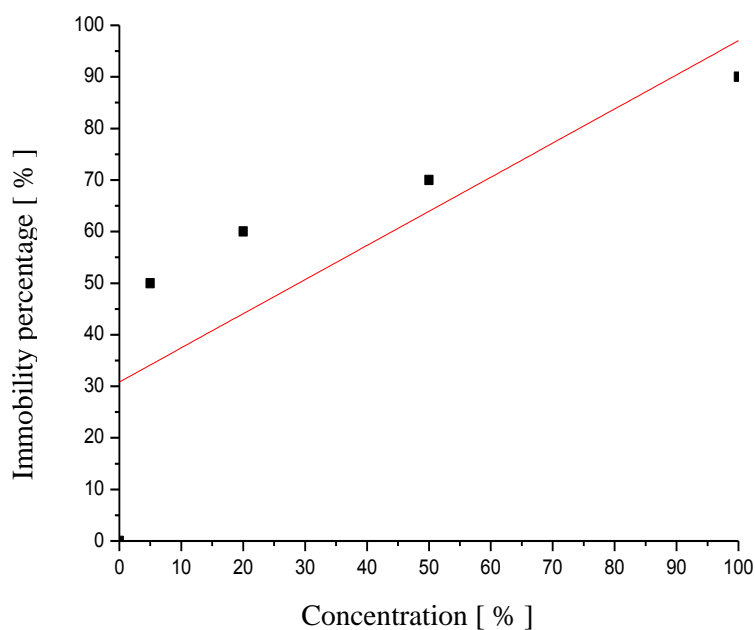| Concentration of solutions treated with blank sample(%)	The number of active *Daphnia magna*	Immobility (Mortality) rate (%)
100	0	100
50	0	100
20	2	80
5	3	70

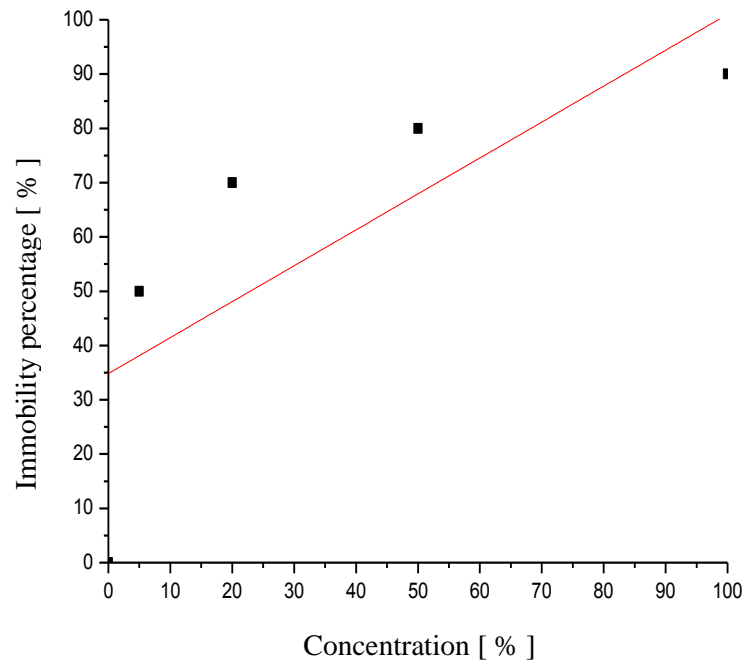Figure 4.23 Concentration vs. immobility diagram of sample 1

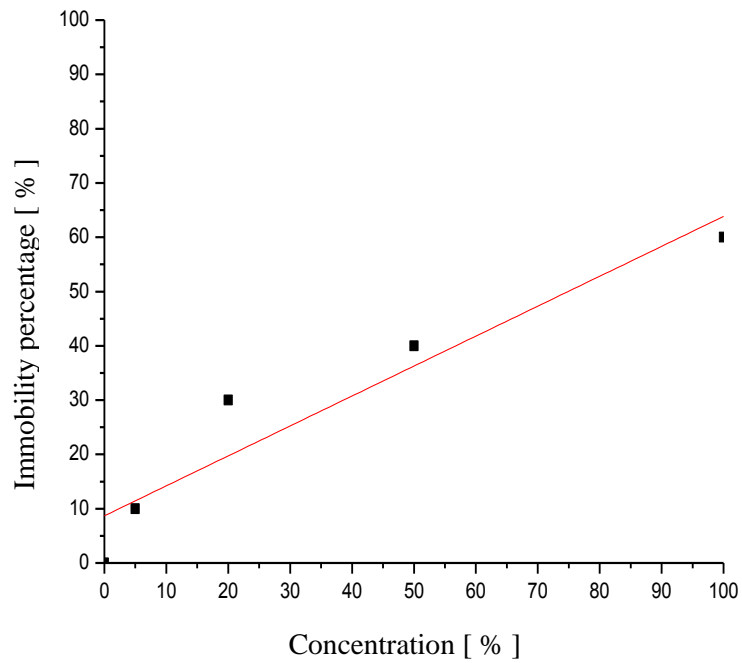Figure 4.24 Concentration vs. immobility diagram of sample 2

Figure 4.25 Concentration vs. immobility diagram of sample 3
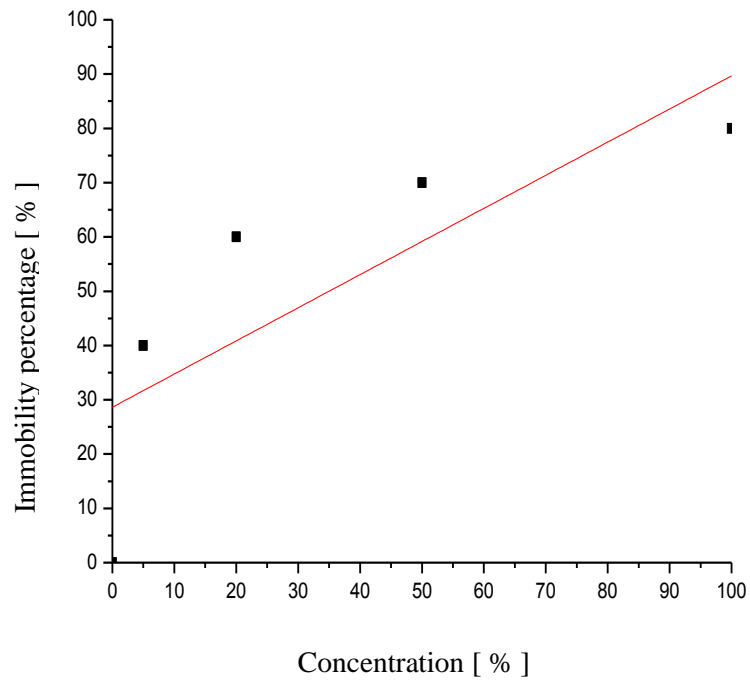
Figure 4.26 Concentration vs. immobility diagram of sample 4
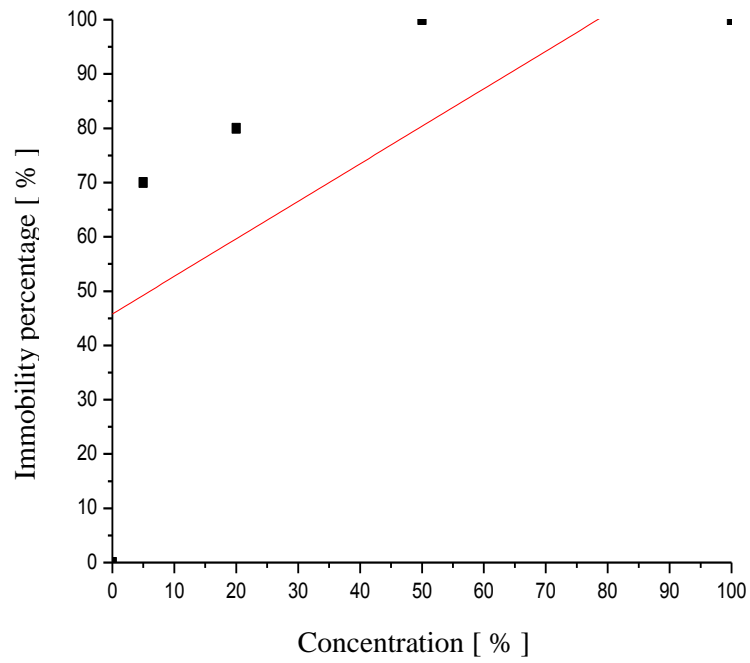
Figure 4.27 Concentration vs. immobility diagram of control sample

The solutions were prepared at 5, 20, 50, 100 percentage dilution rates for treated water with sample 1 and median effective concentration was found to be 28% (Figure 4.23). The solutions were prepared at 5, 20, 50, 100 percentage dilution rates for treated water with sample 2 median effective concentration was found to be 22% (Figure 4.24). The solutions were prepared at 5, 20, 50, 100 percentage dilution rates for treated water with sample 3 and median effective concentration was found to be 76% (Figure 4.25). The solutions were prepared at 5, 20, 50, 100 percentage dilution rates for treated water with sample 4 and median effective concentration was found to be 34% (Figure 4.26). The solutions were prepared at 5, 20, 50, 100 percentage dilution rates for treated water with control sample and median effective concentration was found to be 4% (Figure 4.27).

4.8 Reactor Design

4.8.1 Fundamental Aspects of Reactor Design

To achieve higher degradation efficiency;

- The surface of the reactor was coated with glass , this will led to more photocatalytic degradation efficiency
- Reactor was designed and produced with 40 degree angle to absorb sunlight with right angle.
- To avoid evaporation, reactor was designed closed system. With the help of influent and effluent lid, water can enter and leave the entire system.
- To prevent water to leave the reactor, inner surface of the reactor was totally coated with silicon.

The reactor was designed and produced by using these design parameters.

4.8.2 Experiments of a Prototype Reactor

Reactor was tested as a batch reactor. The photos from prototype reactor is illustrated in Figure 4.28-4.30.In order to achieve higher efficiency, MB water solution was kept 1 hours of reaction time. Influent water was collected in a reactor.

Effluent water was collected and sent to spectrophotometer to measure absorbance values. Degradation results were demonstrated in Table 4.18 and Figure 4.31-4.32.

Figure 4.28 Right side view of the reactor

Figure 4.29 Left side view of the reactor

Figure 4.30 Overhead view of the reactor
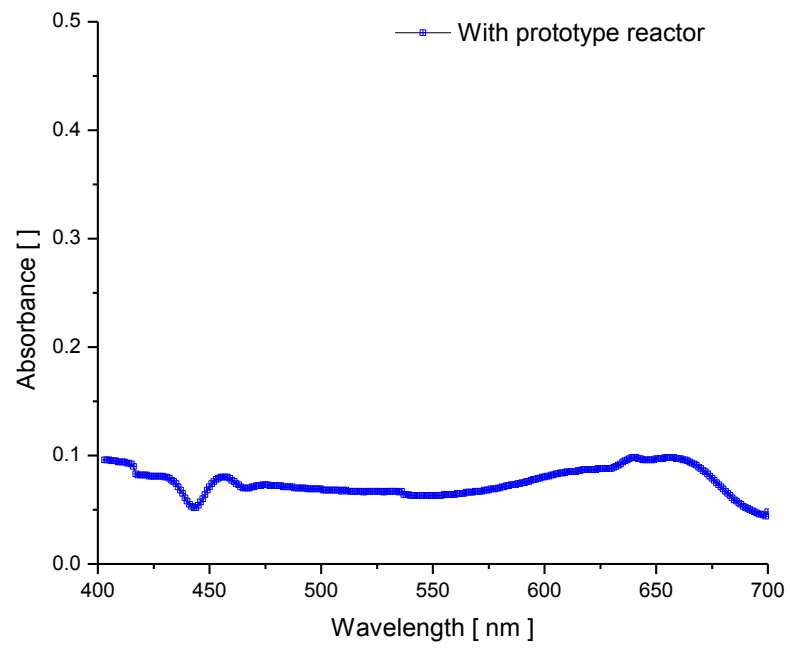
Figure 4.31 Degradation experiment of prototype reactor
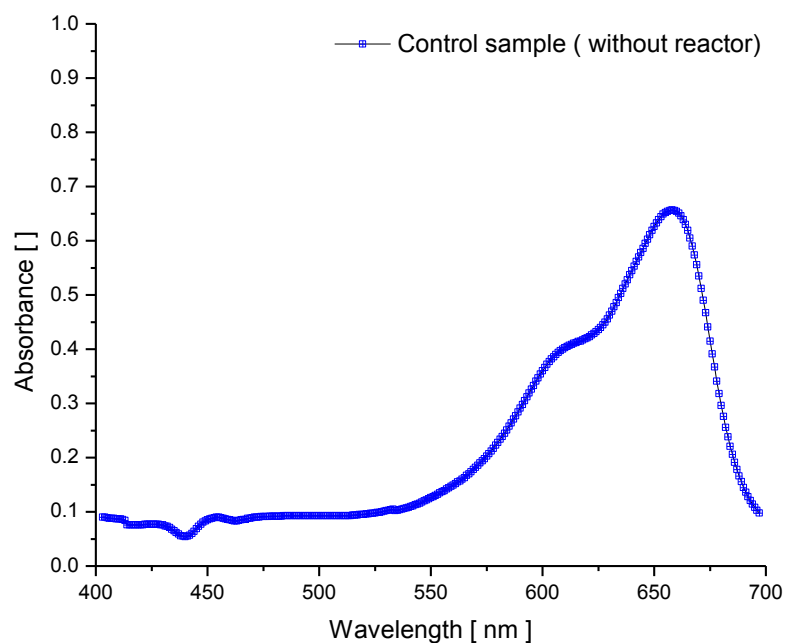
Figure 4.32 Degradation experiment of control sample (without reactor)

Table 4.21 Degradation efficiency results

Material used	Degradation efficiency (%)
Exposed to sunlight with reactor	88%
Exposed to sunlight without reactor	17%

Degradation efficiency calculation was given in equation 3.1

   Subsequently, degradation tests were carried out with prototype reactor and blank sample. As shown in Table 4.21, reactor was reached higher efficiency in a short time and showed 61% more degradation percentage than blank sample. This work will perform preliminary work for future plans and studies. Prototype reactor achieved good degradation and this will lead to use and application of photocatalysts to industries for degradation of dyes.

CHAPTER FIVE
CONCLUSION AND SUGGESTIONS

5.1 General Results

In this thesis, KLTO thin films were successfully produced on silicon substrates and their toxicity and photocatalytic degredation tests were performed. From this study, the obtained results are given in below.

1) The pH of the KLTO solution was found to be 3.51 and this means the solution is acidic. Turbidity value was measured 14.32 ntu and this demonstrated the KLTO based solution was completely dissolved. The color from potassium powder increased the turbidity value.

2) KLTO based thin films performed less toxic effect on *Daphnia magna* acute toxicity test of methylene blue azo-dye and potassium cyanide solution. EC_{50} value of Sm doped KLTO based solution was showed no toxic effect without any dilution. This leads to more photocatalytical degradation and less toxicity. The best photocatalyst can be chosen as Sm doped KLTO. In contrast to these samples with KLTO photocatalysts, blank sample showed 23% of EC_{50} value for acute toxicity of methylene blue, means that 77% of dilution needed to remove of toxicity. The samples having KLTO based coatings significantly more successful than blank sample for degradation and toxicity of methylene blue.

3) According to photocatalytical degradation measurements were performed for organic contaminant, methylene blue dye. In order to determine effect of photocatalyst, photocatalytical measurements were compared and performed with blank sample placed for each experiment.

4) The best photocatalyst was determined as Sm doped KLTO based thin film according to experiments. The highest photocatalytical degradation was reached in pH=10 and 10 minutes of degradation time. Sm doped KLTO was showed best degradation rate nearly in all experiments. Thanks to Sm doped KLTO based

coating, 91% degradation rate was reached in 10 minutes, 750 W/m^2 light intensity and pH=10.

5) The morphology of the KLTO coatings was found to be affected by solution concentration, pH, viscosity, film thickness, coating technique, and heat treatment regime. This film was prepared to have ten layered coating heat treatment regime was including thermal shocks. These thermal shocks caused micro structure to have cracks and pinholes etc.

6) In order to perform application of photocatalyst under sunlight, KLTO thin films were collected in a designed reactor. The methylene blue solution sample was exposed to sunlight in a reactor. This sample was performed 88% photocatalytic degradation rate. In contrast to this degradation rate, blank sample showed 17% degradation rate.

5.2 Suggestions

KLTO based thin films should be investigated in the future works as an application to industry. In order to reach less photocatalytical degradation time, photocatalysts can be coated with different dopants. Industrial-scale reactor can be performed to provide more degradation for industrial treatment works.

REFERENCES

Ameta, R., Benjamin, S., Ameta, A., & Ameta, S. C. (2013). Photocatalytic degradation of organic pollutants: A review. *Materials Science Forum*, *734*, 247-272

Atlas Material Testing (1999). *Suntest CPS+ Manual*, Linsengericht-Altenhaßlau, Germany: Atlas Mtt.

Bakal, F. (2014). *Production, characterization and industrial applications of new generation photocatalytic materials*. Master Thesis, Dokuz Eylül University, İzmir.

Bakuy, Ş. (2009). *Kirli su temizleme uygulamaları için cam altlıklar üzerine Ru-TiO$_2$ ince film üretimi ve fotokatalitik özelliklerinin incelenmesi*. Dokuz Eylul University, Dissertation Thesis, Izmir.

Binning, G., Quate, C. F., & Gerber C. (1986). Atomic force microscope. *Physical Review Letters*, *56*, 930-933.

Boehm, H. P., & Herrmann, M. (1967). Uber die chemie der oberfläche des titandioxids. I. bestimmung des aktiven wasserstoffs, thermische entwässerung und rehydroxylierung. *Zeitschrift für Anorganische und Allgemeine Chemie*, *352*, 156.

Callister, W.D. Jr. (2008). *Materials science and engineering an introduction* (7th ed.), New York: John Wiley & Sons, Inc.

Cao N., Yang M., Zhang Y., Hu J., Ike M., Hirotsuji J., et al. (2009) . Evaluation of wastewater reclamation technologies based on in vitro and in vivo bioassays. *Science of the Total Environment*, *407,* 1588–1597.

Chong, M.N, Jin, B., Chow, C.W.K, & Saint, C. (2010). Recent developments in photocatalytic water treatment technology: A review. *Water Research*, *44*, 2997-3027.

Cui, W., Liu, L., Feng, L., Xu, C., Li, Z., Lü, S., et al., (2006). Preparation of $Pt/K_2La_2Ti_3O_{10}$ and its photo-catalytic activity for hydrogen evolution from methanol water solution. *Science in China Series B*, *49* (2), 162-168.

Dhananjeyan, M.R., Kandavelu, V., & Renganathan, R. (2000). A study on the photocatalytic reactions of TiO_2 with certain pyrimidine bases: effects of dopants (Fe^{3+}) and calcination. *Journal of Molecular Catalysis A: Chemical*, *151*, 217.

Environmental science. (n.d.) Retrieved May 2, 2015, from http:// sls.cuhk.edu.hk/index.php/research/outstanding-research-2/environmental-science

Fabiyi, M.E., & Skelton, R.L. (2000). Photocatalytic mineralisation of methylene blue using buoyant TiO2-coated polystyrene beads. *Journal of Photochemistry and Photobiology*, *132*, 121.

Figueiredo, S. A., Boaventura, R. A., & Loureiro, J. M. (2000). Color removal with natural adsorbents: modeling, simulation and experimental, *Separation and Purification Technology, 20*, 129–141.

Frank, S. N., & Bard, A. J. (1977). Heterogeneous photocatalytic oxidation of cyanide ion in aqueous solutions at titanium dioxide powder. *Journal of the American Chemical Society*, *99* (1), 303–304.

Frank, S. N., & Bard, A. J. (1977).Heterogeneous photocatalytic oxidation of cyanide and sulfite in aqueous solutions at semiconductor powders. *The Journal of Physical Chemistry, 81* (15), 1484–1488.

Fujishima, A., & Honda, K. (1972). Electrochemical photolysis of water at a semiconductor electrode. *Nature*, *37*, 238.

Giwa, A., Nkeonye, O. P., Bello, K. A., & Kolawole, K. A. (2012). Photocatalytic decolourization and degradation of C. I. Basic Blue 41 Using TiO_2 nanoparticles. *Journal of Environmental Protection*, *3*, 1063-1069.

How XPS works. (n.d.). Retrieved April 10, 2015, from http://www.seallabs.com/how-xps-works.html

Huang, Y., Wei, Y., Cheng, S., Fan, L., Li, Y., Lin, J., et al. (2010). Photocatalytic property of nitrogen-doped layered perovskite $K_2La_2Ti_3O_{10}$. *Solar Energy Materials & Solar Cells, 94*, 761–766.

Ikeda, S., Hara, M., Kondo N. J., & Domen K. (1998). Preparation of $K_2La_2Ti_3O_{10}$ by polymerized complex method and photocatalytic decomposition of water. *Chemistry of Materials*, *10*, 72-77.

Immich, A. P. S., Souza, A. A. U., & Souza, S. M. A. G. U. (2009). Removal of Remazol Blue RR dye from aqueous solutions with Neem leaves and evaluation of their acute toxicity with *Daphnia magna. Journal of Hazardous Materials*, *164*, 1580–1585.

Kodama, F., & Suzuki, J., (2007). How Japanese Companies have used scientific advances to restructure their business: The receiver-active national system of innovation. *World Development*, *35* (6), 976-990.

Miller, J. D., Veeramasuneni, S., Drelich, J., & Yalamanchili, M. R. (1996). Effect of roughness as determined by atomic force microscopy on the wetting properties of ptfe thin films. *Polymer Engineering And Science*, *36* (14), 1849-1855.

Mills, A., & Hunte, S.L. (1997). An overview of semiconductor photocatalysis.*Journal of Photochemistry and Photobiology A:Chemisty*, *108*, 1–35.

Nimetoğlu, Z. (2011). *Yeni nesil fotokatalitik filmlerin üretilmesi ve atıksulardaki organik kirleticilerin temizlenmesinde kullanılması*. Disertation Thesis, Dokuz Eylül University, Izmir.

Pelaez, M., Nolan N. T., Pillai S. C., Seery M. K., Falaras P., Kontos A. G., et al. (2012). A review on the visible light active titanium dioxide photocatalysts for environmental applications. *Applied Catalysis B: Environmental*, *125*, 331–349.

Rand, G. M. (1995). *Fundamentals of aquatic toxicology: Effects environmental fate and risk assessment* (2nd ed.) Florida:Taylor & Francis.

Riera-Torres, M., Gutierrez-Bouzan, C., & Crespi, M. (2010). Combination of coagulation–flocculation and nanofiltration techniques for dye removal and water reuse in textile effluents. *Desalination*, *252*, 53.

Rubo A., Kellens R., Reddy J., Wooten J., & Hasenpusch W. (2006). *Alkali metal cyanides. ullmann's encyclopedia of industrial chemistry*, Weinheim, Germany: Wiley-VCH

Seah, M. P., Gilmore, I. S., & Spencer, S. J. (2001). Analysis of X-ray photoelectron intensities from elemental data in a digital photoelectron database. *Journal of Electron Spectroscopy and Related Phenomena*, *120*, 93–111.

Stolz, A. (2001). Basic and applied aspects in the microbial degradation of azo dyes. *Applied Microbiology and Biotechnology, 56,* 69-80.

Takata, T., Shinohara K.,Tanaka A., Hara M., Kondo J.N., & Domen K. (1997). A highly active photocatalyst for overall water splitting with a hydrated layered

perovskite structure. *Journal of Photochemistry and Photobiology A: Chemistry*, *106,* 45-49.

Ollis, D. F. & Al-Ekabi, H. (1993). Photocatalytic purification and treatment of water and air. *Elsevier Science Publishers*.

Ou, Y., Lin, J.D., Zou, H.M., & Liao, D.W. (2005). Effects of surface modification of TiO_2 with ascorbic acid on photocatalytic decolorization of an azo dye reactions and mechanisms. *Journal of Molecular Catalysis A: Chemical*, *241*, 59.

United States Environmental Protection Agency (USEPA) (1985). *Methods for measuring the acute toxicity of effluent to freshwater and marine organisms* (3rd ed.) Washington, DC: USEPA, United States Environmental Protection Agency.

Wilde, F. D., & Gibs, J. (1998). Turbidity. *Geological survey*, TWRI Book 9 (1-30).

Yang, Y., Chen, Q., Yin, Z., & Li, J. (2009). Study on the photocatalytic activity of $K_2La_2Ti_3O_{10}$ doped with vanadium (V). *Journal of Alloys and Compounds*, *488*, 364–369.

Yao, J., & Wang, C. (2010). Decolorization of methylene blue with TiO_2 sol via UV irradiation photocatalytic degradation. *International Journal of Photoenergy*, (1), 6-12.

Yiğit, Z. (2008). *Fotokatalitik arıtmanın doğal organik madde karakterizasyonu ve dezenfeksyon yan ürünlerine etkisi*. Master Thesis, Graduate School of Natural and Applied Sciences of Anadolu University, Eskişehir.